RESEARCH PAPER

Reliability-based multi-scale design optimization of composite frames considering structural compliance and manufacturing constraints

Zunyi Duan[1,2] · Yongsu Jung[2] · Jun Yan[3] · Ikjin Lee[2]

Abstract

The paper proposes an efficient methodology for concurrent reliability-based multi-scale design optimization (RBMDO) of composite frames to minimize structural cost subjecting to compliance constraint. Two types of variables are systematically considered in RBMDO, which are deterministic design variables of the frame components, the discrete fiber winding angles at the two geometrical scales, and random parameters of material properties and loading conditions in both magnitude and direction. To overcome the difficulty of highly nonlinear compliance constraint when using fiber winding angles as design variables and improve efficiency and accuracy of RBMDO of composite frames, the improved single loop and single vector (SLSV) approach based on modified chaos control (MCC) scheme, which is abbreviated hereafter as SLSV-MCC, is proposed, and sensitivities at the current design point are utilized to further increase accuracy of the proposed SLSV-MCC. Six types of specific manufacturing constraints are explicitly considered in the proposed RBMDO to reduce the risk of local failure in the laminated composite. The deterministic multi-scale design optimization (DMDO) model is also presented and utilized for comparison to distinguish differences between deterministic and reliability-based optimization results. Efficiency and accuracy of the proposed SLSV-MCC are compared with the first-order reliability method (FORM) and conventional SLSV approach. Meanwhile, the Monte Carlo simulation (MCS) method is further utilized to validate the accuracy of the proposed RBMDO. The discrete material optimization (DMO) approach is utilized to couple two geometrical scales: macroscopic topology and microscopic material selection. Capabilities of the proposed RBMDO are demonstrated by optimization of 2D and 3D composite frames. Numerical study reveals that the uncertainties in material properties and loading conditions will lead to different macroscopic sizing and topology configurations for deterministic and reliability-based solutions.

Keywords Reliability-based design optimization · Concurrent multi-scale design optimization · Discrete material optimization · Single loop single vector · Modified chaos control

---

Responsible Editor: Jianbin Du

✉ Zunyi Duan
  duanzy@nwpu.edu.cn

✉ Ikjin Lee
  ikjin.lee@kaist.ac.kr

1 Institute of Structural Health Monitoring and Control, School of Mechanics, Civil Engineering & Architecture, Northwestern Polytechnical University, Xi'an 710072, China

2 Department of Mechanical Engineering, Korea Advanced Institute of Science and Technology, Daejeon 34141, Republic of Korea

3 Department of Engineering Mechanics, State Key Laboratory of Structural Analysis for Industrial EquipmentInternational Research Center for Computational Mechanics, Dalian University of Technology, Dalian 116024, Liaoning, China

1 Introduction

Concurrent multi-scale design optimization provides a competitive approach to realize innovative structure configuration and lightweight design through macro-scale structural topology and micro-scale material selection. Pioneering work of the multi-scale optimization on hierarchical structure and material design is found in Rodrigues et al. (2002). Then, the hierarchical model has been extended to investigate concurrent material and topology optimization of three-dimensional structures and bone tissue adaptation (Coelho et al. 2008). State-of-the-art researches for multi-scale design optimization of structures with cellular and porous material can be found in Liu et al. (2008), Yan et al. (2008), Niu et al. (2009), Zuo et al.

(2013), Andreasen and Sigmund (2012), and Deng et al. (2013).

Laminated fibrous composite materials have been widely used, especially in aerospace, automotive, advanced shipping, and civil engineering, due to their superior material properties for high specific strength and stiffness. As architecture material, laminated composites offer a good opportunity to tailor the material properties by adjusting the fiber ply parameters. Thus, many researchers have recently carried out excellent works on multi-scale lightweight design optimization of composite structures. Ferreira et al. (2013) adopted the DMO (Stegmann and Lund 2005; Hvejsel and Lund 2011) approach to perform a hierarchical optimization of laminated composite structures considering both fiber orientation and cross-section size/shape. For more researches about the deterministic multi-scale design optimization (DMDO) of composite material and structure, readers can refer to Gao et al. (2013), Sørensen et al. (2014), Duan et al. (2015), Yan et al. (2017), Duan et al. (2018, 2019a, b), Wu et al. (2019) and Ma et al. (2020).

Uncertainties are inevitable and pervasive in simulation, modeling, manufacturing processes, material properties, and loading environments. Without considering uncertainties in optimization, the optimum design will have a high risk of failure. Hence, reliability-based design optimization (RBDO) has been applied to structural design optimization with multi-scale materials such as laminated composites to guarantee reliability and robustness (Guo et al. 2009; 2015; António and Hoffbauer, 2009; Deng and Chen 2017; Shimoda et al. 2019). Recently, it should be pointed out that Sohouli et al. (2018) investigated RBMDO of variable stiffness composite structures with sequential optimization and reliability assessment (SORA), and hybrid RBDO decoupled scheme to determine material and fiber orientation. Xu et al. (2019) proposed a non-deterministic robust topology optimization of ply orientation for multiple fiber-reinforced plastic (FRP) materials under loading uncertainties with both random magnitude and random direction.

Efficient but accurate reliability analysis needs to be performed in reliability-based multi-scale design optimization (RBMDO) of composite structures with many deterministic and random design variables. Commonly, reliability analysis is classified into two types: (1) sampling methods such as MCS (Papadrakakis and Lagaros 2002; Cho et al. 2016), importance sampling (IS) (Denny 2001), and latin hypercube sampling (Helton and Davis 2003) and (2) analytical methods or most probable point (MPP)-based methods including first-order reliability method (FORM) (Chiralaksanakul and Mahadevan 2005; Shin and Lee 2014), second-order reliability method (SORM) (Kiureghian et al. 1987; Lee et al. 2012), and MPP-based dimension reduction method (Lee et al. 2008, 2010; Kang et al. 2017; Jung et al. 2019). Recently, Imani et al. (2018, 2019) investigated general nonlinear state-space and data-poor environment problems with Bayesian method. Xie et al. (2017) proposed a linear discriminant analysis classification rule to investigate

nonstationary data problem. To improve the computational efficiency of conventional RBDO, Chen et al. (1997) proposed the single loop single vector approach (SLSV), and Jeong and Park (2017) improved SLSV by proposing the single loop single vector conjugate gradient (SLSVCG) approach using the conjugate gradient at MPP of the previous cycles.

There are three major challenges in applying RBMDO to composite frames: (1) the number of design variables dramatically increases as the number of components in the composite frames increases since both cross-sections of the beams in the macro-scale and fiber winding angles in the micro-scale are considered as independent design variables in RBMDO. (2) When fiber winding angles are used as design variables directly, the convexity of the objective function is not guaranteed (Foldager et al. 1998; Duan et al. 2019a, b), which may lead to instability and inaccuracy in convergence during reliability analysis. (3) In practical applications, design guidelines or rules, referred to as manufacturing constraints, must be considered to reduce local failure risk in the composite structure (Bailie et al. 1997; Yan et al. 2017).

Consequently, the purpose of this paper is to propose an efficient RBMDO for composite frames under uncertainties in material properties and loading conditions. To enhance the stability of structural performance in a real operational environment, load uncertainties in both magnitude and direction are considered in RBMDO. The DMO approach for multi-scale optimization of laminated composites is adopted in RBMDO of composite frames to overcome the non-convexity and high non-linearity. Based on MCC scheme (Yang and Yi 2009; Meng et al. 2015), the SLSV-MCC approach which utilizes sensitivities at the current design point is proposed for more efficient RBMDO of composite frames with manufacturing constraints.

The rest of the paper is organized as follows. Review of RBDO related to the proposed method is presented in Sect. 2. The proposed SLSV-MCC is explained in Sect. 3. Concept and mathematical formulation of RBMDO are introduced along with DMDO in Sect. 4. Section 5 presents the parameterization of the DMO approach and sensitivity analysis for the proposed RBMDO. Explicit mathematical expressions for specific manufacturing constraints as well as two solution strategies are briefly described in Sect. 6. Numerical study with 2D and 3D composite frames is performed using RBMDO and DMDO in Sect. 7. Finally, Sect. 8 concludes the paper.

2 Review of reliability-based design optimization

2.1 Reliability-based design optimization

In comparison with deterministic design optimization, RBDO takes into account uncertainties for variables and parameters

that may influence the structural response. In the present research, RBDO with random parameters and deterministic design variables can be mathematically formulated as

$$\min_{\boldsymbol{d}} C(\boldsymbol{d}) \, Subject \, to : \begin{cases} Pr[G_l(\boldsymbol{d},\boldsymbol{P}) > 0] \leq P_{f_l}^{Tar} \, (l = 1 \cdots nc) \\ \boldsymbol{d}^L \leq \boldsymbol{d} \leq \boldsymbol{d}^U \end{cases} \quad (1)$$

where $C(\boldsymbol{d})$ is the objective function; $\boldsymbol{d}$ is the deterministic design variable vector with the upper bounds $\boldsymbol{d}^U$ and lower bounds $\boldsymbol{d}^L$, the design spaces of $\boldsymbol{d}$ are the macro-scale inner tube radius and micro-scale artificial material density in the two geometrical scales in this paper; $\boldsymbol{P}$ represents the random vector; $Pr[\cdot]$ is the probability function; $P_{f_l}^{Tar}$ is the target probability of failure for the l-th constraint; nc is the number of the limit functions or probabilistic constraints; and $G_l(\boldsymbol{d},\boldsymbol{P})$ is the l-th limit state function such that $G_l(\boldsymbol{d},\boldsymbol{P}) > 0$ is defined as failure. The purpose of RBDO is to find the optimum that the probability of failure in each constraint has to be less than the target probability of failure. In (1), the probability of failure in reliability analysis can be calculated using a multi-dimensional integral as

$$P_f \equiv Pr[G_l(\boldsymbol{d},\boldsymbol{P}) > 0] = \int \cdots \int_{G(\boldsymbol{d},\boldsymbol{P}) > 0} f_{\boldsymbol{P}}(\boldsymbol{p}) d\mathbf{p} \quad (2)$$

where P_f is the probability of failure and $f_{\boldsymbol{P}}(\boldsymbol{p})$ is the joint probability density function (PDF) of random parameter $\boldsymbol{P}$. The limit-state function is generally transformed from the original space (X-space) to the standard normal space (U-space) (Rosenblatt 1952) for easy integration. Then, the integration in (2) can be rewritten as

$$P_f = Pr[G_i(\boldsymbol{d},\boldsymbol{P}) > 0] = \int \cdots \int_{g(\boldsymbol{u}) > 0} f_{\boldsymbol{U}}(\boldsymbol{u}) d\mathbf{u} \quad (3)$$

where $f_{\boldsymbol{U}}(\boldsymbol{u})$ is the joint PDF of the standard normal variables U and $g(\boldsymbol{u})$ is the limit-state function in U-space. For efficient computation of (3), FORM linearizes $g(\boldsymbol{u})$ at $\boldsymbol{u}^*$, which is MPP in U-space obtained through the Rosenblatt transformation, as

$$g(\boldsymbol{u}) \cong g(\boldsymbol{u}^*) + \nabla g^T(\boldsymbol{u}^*)(\boldsymbol{U} - \boldsymbol{u}^*) \quad (4)$$

where $\nabla g^T(\boldsymbol{u}^*)$ is the gradient of $g(\boldsymbol{u})$ at $\boldsymbol{u}^*$ and T stands for transpose. $\boldsymbol{u}^*$ is obtained by solving

$$\min_{\boldsymbol{u}} \|\boldsymbol{u}\| \, Subject \, to : g_l(\boldsymbol{u}) = 0 \, (l = 1 \cdots nc) \quad (5)$$

A reliability index β_l is defined as the distance from the origin to $\boldsymbol{u}^*$, that is,

$$\beta_l = \|\boldsymbol{u}^*\| = \left(\boldsymbol{u}^{*T}\boldsymbol{u}^*\right)^{1/2} \quad (6)$$

FORM estimates the probability of failure using the reliability index as $\Phi(-\beta_l)$.

Using performance measure approach (PMA) (Youn et al. 2003), (5) can be rewritten to find MPP as

$$\max_{\boldsymbol{u}} g_l(\boldsymbol{u}) \, Subject \, to : \|\boldsymbol{u}\| = \beta_l^t = -\Phi^{-1}\left(P_{f_l}^{Tar}\right) \quad (7)$$

where β_l^t is the target reliability index obtained from the target probability of failure $P_{f_l}^{Tar}$. By applying the Lagrange multiplier method in (7), the general updating formula for MPP search is derived as

$$\boldsymbol{u}^{(\varsigma+1)} = \beta_l^t \frac{\nabla g(\boldsymbol{u}^{(\varsigma)})}{\|\nabla g(\boldsymbol{u}^{(\varsigma)})\|} \quad (8)$$

where ς is the iteration for MPP search.

2.2 Single loop single vector approach

To eliminate the inner loop, that is, the reliability analysis loop for MPP search, SLSV approximates MPP by utilizing the sensitivity of a performance function in the previous design (Chen et al. 1997), and thus, the MPP updating formula in (8) can be replaced in SLSV as

$$\boldsymbol{u}^{(\varsigma)} = \boldsymbol{\mu}_{\boldsymbol{p}} + \beta_l^t \boldsymbol{\sigma}_{\boldsymbol{p}}^T \boldsymbol{\alpha}^{(\varsigma-1)} \, where \, \boldsymbol{\alpha}^{(\varsigma-1)} = \frac{\boldsymbol{\sigma}_{\boldsymbol{p}}^T \nabla g(\boldsymbol{u}^{(\varsigma-1)})}{\left\|\boldsymbol{\sigma}_{\boldsymbol{p}}^T \nabla g(\boldsymbol{u}^{(\varsigma-1)})\right\|} \quad (9)$$

where $\boldsymbol{\mu}_{\boldsymbol{p}}$ and $\boldsymbol{\sigma}_{\boldsymbol{p}}$ are the mean vector of $\boldsymbol{p}$ and the standard deviation of $\boldsymbol{p}$, respectively. Since the approximated MPP is found using the gradient from the previous design, MPP search iteration is not necessary in SLSV. Therefore, SLSV significantly improves computational efficiency of RBDO by eliminating the inner loop. RBDO using SLSV is formulated as

$$\min_{\boldsymbol{d}} Cost(\boldsymbol{d}) \, Subject \, to : \begin{cases} g_l\left(\boldsymbol{d}, \boldsymbol{p}_{l,MPP}^{(k)}\right) \leq 0 \, (l = 1 \cdots nc) \\ \boldsymbol{p}_{l,MPP}^{(k)} = \boldsymbol{\mu}_{\boldsymbol{p}} + \beta_l^t \boldsymbol{\sigma}_{\boldsymbol{p}}^T \boldsymbol{\alpha}_l^{(k-1)} \\ \boldsymbol{\alpha}_l^{(k-1)} = \left[\frac{\boldsymbol{\sigma}_{\boldsymbol{p}}^T \nabla g_l(\boldsymbol{u}^{(k-1)})}{\left\|\boldsymbol{\sigma}_{\boldsymbol{p}}^T \nabla g_l(\boldsymbol{u}^{(k-1)})\right\|}\right]_{\boldsymbol{p}=\boldsymbol{p}_{l,MPP}^{(k-1)}} \\ \boldsymbol{d}^L \leq \boldsymbol{d} \leq \boldsymbol{d}^U \end{cases} \quad (10)$$

where $\boldsymbol{p}_{l,MPP}^{(k-1)}$ is the MPP at the $(k$-$1)$-th iteration for the l-th constraint and $\boldsymbol{\alpha}_l^{(k-1)}$ is the normalized gradient vector of the l-th constraint. Due to the MPP approximation, the number of function evaluations in SLSV may be similar with computational demands in deterministic optimization. However, the approximation may cause large error and divergence in case of highly nonlinear performance functions because exact MPP search is replaced with the approximation by gradient vector of previous MPP. Therefore, these difficulties need to be alleviated while maintaining the advantages of SLSV.

3 Improved SLSV for efficient RBDO

As discussed in Sect. 2.2, one of the weaknesses in the single loop RBDO using SLSV is inaccurate MPP approximation for highly nonlinear performance functions. To maintain efficiency of SLSV and overcome its inaccuracy, the modified SLSV based on MCC is proposed to solve concurrent multi-scale design optimization of composite frame where uncertain parameters such as material properties and loading conditions are considered, and the cross-sections of the beam at the macro-scale and the discrete fiber winding angles at the micro-scale are deterministic. Accordingly, since only random parameters exist in the design formulation, the gradient of a performance function with respect to the random parameter is not necessary for an optimizer since it is invariant during the optimization. SLSV is modified to utilize the sensitivity obtained in current design point without requiring additional function evaluations, and the concept of MCC is adopted to increase the accuracy of reliability analysis.

3.1 Improved SLSV approach based on MCC

To overcome the convergence problem in reliability analysis for highly nonlinear functions, Yang and Yi (2009) proposed the chaos control (CC) method. With considering the weakness of CC in convex or concave performance measure functions, Meng et al. (2015) proposed MCC by extending the iterative point of the CC method to the constraint boundary to investigate double-loop RBDO. Some new developments of MCC can be found in Keshtegar et al. (2017) and Yang et al. (2018) where the self-adaptive modified chaos control (SMCC) method and the accelerated stability transformation method (ASTM) of chaos control are proposed, respectively. In this research, the SLSV-MCC approach is proposed to fully exploit the potential of MCC and SLSV on accuracy and efficiency, respectively. In MCC, new direction of MPP is estimated as

$$\widetilde{n}(u^{\varsigma+1}) = u^{\varsigma} + \lambda C(f(u^{\varsigma}) - u^{\varsigma}), 0 < \lambda < 1 \qquad (11-a)$$

$$u^{\varsigma+1} = \beta_l^t \frac{\widetilde{n}(u^{\varsigma+1})}{\left\| \widetilde{n}(u^{\varsigma+1}) \right\|} \qquad (11-b)$$

where

$$f(u^{\varsigma}) = -\beta_l^t \frac{\nabla_U g(d, u^{\varsigma})}{\|\nabla_U g(d, u^{\varsigma})\|} \qquad (12)$$

where a stabilization factor λ is determined according to eigenvalues of the original system's Jacobian matrix, and C is the involutory matrix with only one element in each row and size of n × n where n is the number of random variables. In this study, an identity matrix is selected for C, and λ is set to be 0.7

based on heuristically. Note that the superscript ς in (12) stands for the iteration in MPP search.

By adopting the concept of MCC with the stabilization factor λ in SLSV, the MPP updating formula in (10) can be rewritten in the proposed SLSV-MCC as

$$u^k = \mu_p + \beta_t \sigma^T \widetilde{n}(u^k) \qquad (13)$$

where

$$\widetilde{n}(u^k) = u^{(k-1)} + \lambda C(f(u^k) - u^{k-1}) \qquad (14)$$

and

$$f(u^k) = -\beta_t \left[\frac{\nabla_U g(d^k, u^{k-1})}{\|\nabla_U g(d^k, u^{k-1})\|} \right]_{u=u_{MPP}^{(k-1)}} \qquad (15)$$

Note that k is iteration for design optimization of SLSV-MCC. Since SLSV has a single loop for design optimization without inner loop for MPP search, deterministic design variable d is changed as the optimization proceed denoted as superscript. Hence, MPP is approximated in the SLSV-MCC using the gradient at the current MPP denoted as $\nabla_U g(d^k, u^{k-1})\big|_{u=u_{MPP}^{(k-1)}}$ and the previous MPP vector denoted as u^{k-1}.

Figure 1 illustrates differences between conventional SLSV and the proposed SLSV-MCC specialized for RBDO problems with random parameters only. There are two major differences compared with conventional SLSV: (1) utilization of gradient when deterministic design vector is d^k instead of d^{k-1} and (2) application of stabilization factor λ with MCC approach to prevent significant error on estimating MPP induced by high nonlinearity. In Fig. 1, k means the iteration number for single-loop optimization. Specifically, k-th MPP is approximated by the gradient obtained from the $(k-1)$-th iteration in conventional SLSV. However, in this research, the gradient obtained in the k-th iteration can be directly used since there is no random design variable. Meanwhile, to avoid oscillation in MPP search and increase accuracy, the stabilization factor used in MCC is adopted. Hence, the approximated MPP based on the previous MPP vector and gradient at the current MPP by SLSV is obtained as shown in Fig. 1b.

The advantage of using the gradient vector in k-th iteration rather than $(k-1)$-th iteration is the improvement of better approximation on MPP. However, the gradient of performance on current design point cannot be applied without further function evaluations if random design variables exist since sensitivity analysis is required at MPP.

3.2 Process of SLSV-MCC

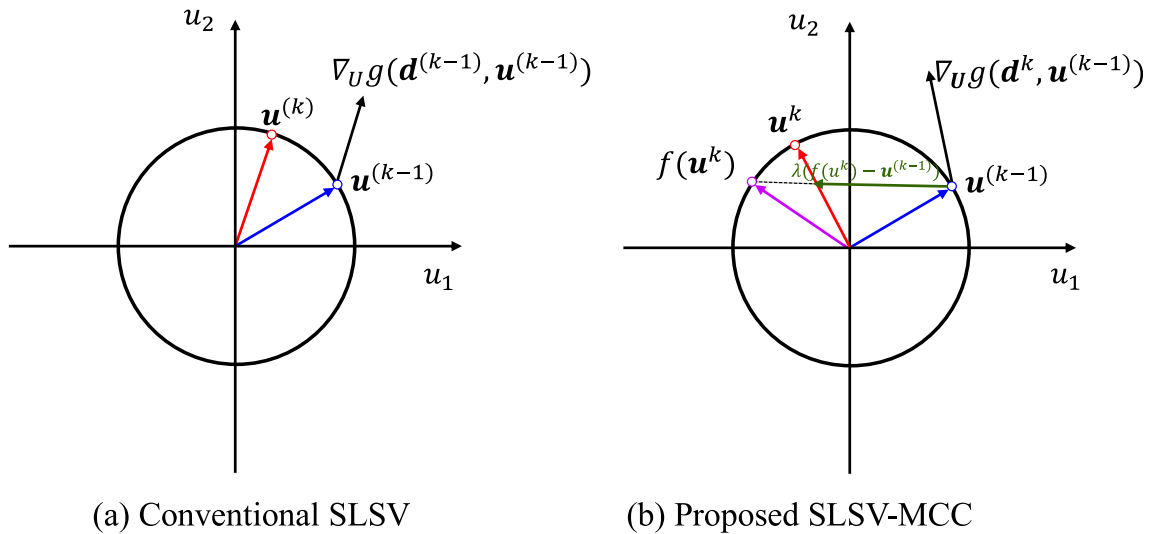The main difference between SLSV and SLSV-MCC is how to obtain a new MPP using gradient vectors as shown in green

(a) Conventional SLSV   (b) Proposed SLSV-MCC

Fig. 1 Approximation of MPP at each design point: **a** conventional SLSV and **b** proposed SLSV-MCC

boxes of Fig. 2 which shows a detailed procedure for SLSV and SLSV-MCC. In SLSV, the new MPP is approximated by the previous information only, and in the proposed SLSV-MCC, sensitivity analysis with respect to random parameters at the current design point is performed in prior to approximate the new MPP by MCC. Notably, the number of function
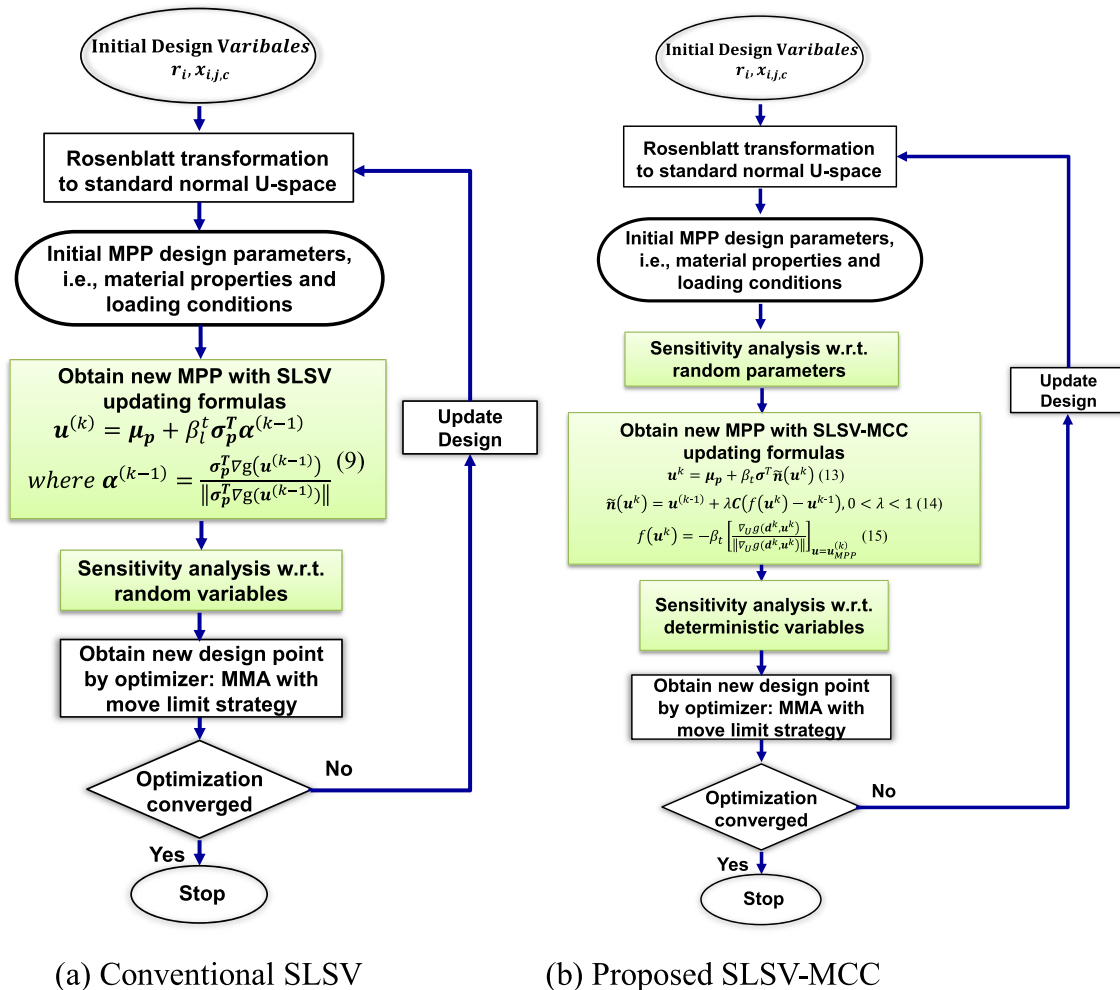

(a) Conventional SLSV   (b) Proposed SLSV-MCC

Fig. 2 Flowchart of **a** SLSV and **b** proposed SLSV-MCC

evaluations required in both algorithms is identical since there is no random variable.

4 Reliability-based multi-scale design optimization of composite frames

4.1 Concept of RBMDO

The concept of RBMDO under uncertainties related to material properties and loading conditions is shown in Fig. 3.

In the macroscopic level as shown in the left part of Fig. 3, load uncertainties in both magnitude and direction are considered in this study to consider a real operational environment. The inner radii of circular cross-sections (r_i as shown in Fig. 3) of beam components in the frame are considered as macroscopic deterministic design variables. The ground structure approach (Bendsøe and Sigmund 2013) is adopted where the tube is deleted from the original ground frame structure when its radius reaches the specified lower limit. Thus, both sizing and topology optimization of macroscopic structural configuration can be achieved.

In the microscopic level as shown in the right part of Fig. 3, composite material properties, i.e., longitudinal stiffness E_{11}, transverse modulus E_{22}, and shear modulus G_{12}, are considered to be random parameters since they have the strongest relation with structure compliance as pointed by Sohouli et al. (2018). The DMO approach, which will be explained in Sect. 5.1, is adopted in the microscopic level to realize selection of discrete fiber winding angles to overcome difficulty of non-convexity and high non-linearity when the fiber winding angles are directly recognized as design variables. Considering cost and process requirements, the most commonly used discrete fiber ply angles in industrial applications, i.e., $[0^{\circ}, \mp 45^{\circ}, 90^{\circ}]$, are adopted. Composite tubes are mostly manufactured by filament winding process (Martins et al. 2014). Mallick (2007) suggested that 0° and 90° fiber winding angles in the filament winding process should be implemented by 5° and 85° fiber winding angles, respectively. In this paper, assembly

of $[5^{\circ}, \mp 45^{\circ}, 85^{\circ}]$ is considered as a set of candidate composite fiber winding angles. The fiber winding angle is assumed to be constant in a given ply. It should be noted that the joints connecting composite tubes can transfer moments, and are assumed to be infinitely stiff for the composite frames in this study.

4.2 Mathematical formulation for DMDO and RBMDO of composite frames

Mathematical formulations of DMDO and RBMDO for composite frames to minimize structural cost while satisfying structural compliance and manufacturing constraints are explained in this section. For both DMDO and RBMDO, manufacturing constraints ($MC1 - MC6$) which will be briefly explained in Sect. 6.1 are considered and it is assumed that damping is neglected. The convergence measure given in Stegmann and Lund (2005) and explained in Appendix A is utilized for the convergence criterion in this study. As shown in Fig. 3, the macro-scale inner tube radius (r_i) and micro-scale artificial material density ($x_{i,j,c}$) related to discrete fiber winding angles are set to be independent design variables to realize topology and stacking sequence optimization of the two geometrical scales simultaneously. Thus, DMDO for composite frames can be formulated as

$$\min_{r_i} V(r_i) = \sum_{i=1}^{N^{\text{tub}}} \pi \left[\widetilde{t_i^{tot}}^2 + 2r_i \widetilde{t_i^{tot}} \right] L_i$$

$$\text{Subject to}: \begin{cases} C\left(UK\left(D_n^e\left(r_i, x_{i,j,c}\right)\right)U\right) \le C^{Tar} \\ \text{S.T.} K\left(D_n^e\left(r_i, x_{i,j,c}\right)\right)U = F \\ r_i \in [r_{\min}, r_{\max}] \\ x_{i,j,c} \in [0,1] \\ i = 1, 2, ..., N^{\text{tub}}, j = 1, 2, ..., N^{\text{lay}}/2, c = 1, 2, ..., N^{\text{can}} \\ \text{Manufacturing Constraints } (MC1-MC6) \end{cases} \quad (16)$$

where V is the structure cost of the composite frames; r_i is the inner radius of the composite tube; t_i^{tot} and L_i are the current total thickness after punishment as presented in Sect. 6.2.2 and
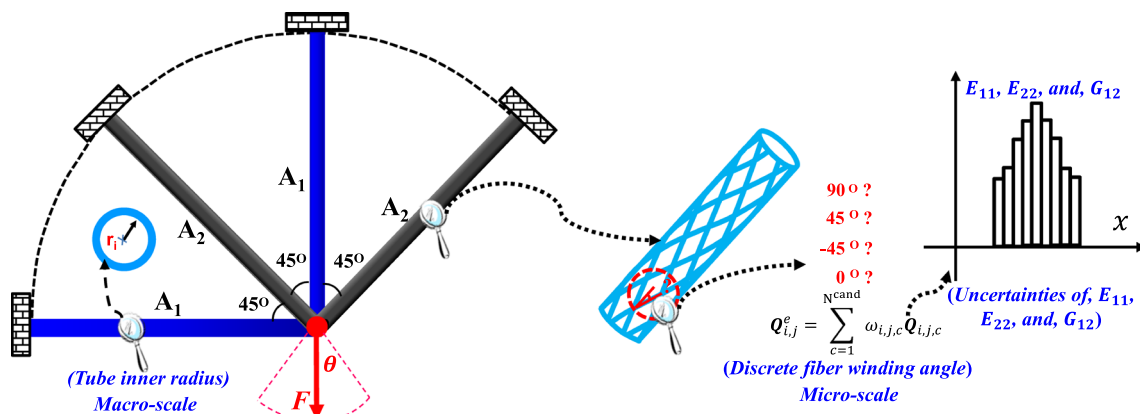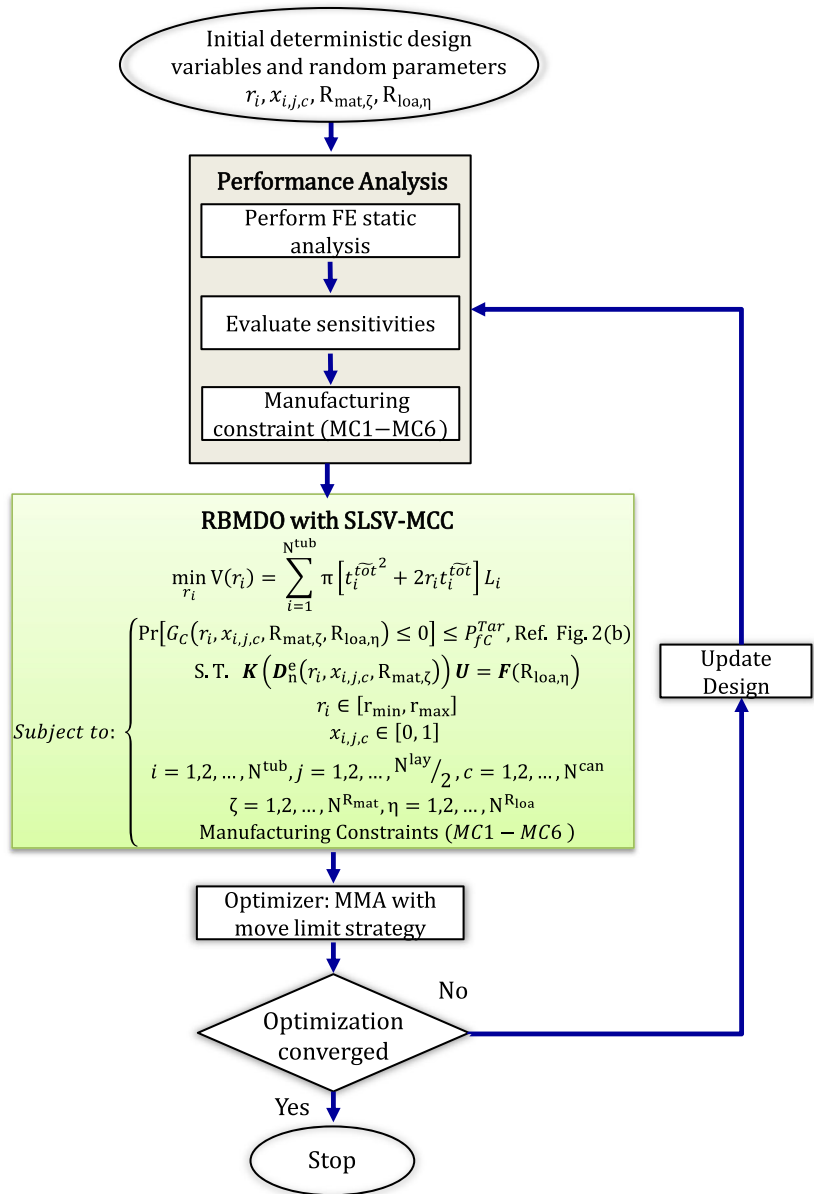

Fig. 3 Schematic diagram of RBMDO of composite frames (adapted from Duan et al. 2019a, b)

Fig. 4 Flowchart of RBMDO with SLSV-MCC in design optimization of composite frames under structural compliance and manufacturing constraints

Table 1 Material properties of the uni-directional CFRE

Property of CFRE	Symbol	Value	Unit
Longitudinal modulus	E_{11}	1.43×10^{11}	Pa
Transverse modulus	$E_{22} = E_{33}$	1.0×10^{10}	Pa
In-plane shear modulus	G_{12}	6.0×10^{9}	Pa
In-plane shear modulus	G_{13}	5.0×10^{9}	Pa
Transverse shear modulus	G_{23}	3.0×10^{9}	Pa
Major Poisson's ratio	υ_{12}	0.3	–
Major Poisson's ratio	υ_{13}	0.2	–
Minor Poisson's ratio	υ_{23}	0.52	–
Mass density	ρ_{carbon}	1800	kg/m³

length of the i-th tube, respectively; $x_{i,\,j,\,c}$ is the artificial density of DMO candidate materials whose subscripts i, j, and c denote the number of tubes, layers, and candidate materials, respectively; C and C^{Tar} denote the structure compliance and its target, respectively; U and K are the displacement vector and stiffness matrix; D_n^e is the element constitutive matrix for the n-th element; N$^{\text{tub}}$, N$^{\text{lay}}$, and N$^{\text{cand}}$ denote the total number of tubes, layers, and candidate materials, respectively; the ground structure approach (Bendsøe and Sigmund 2013) is adopted to realize the topology optimization. The lower bound on the inner radius, r$_{\text{min}}$, is set to be 0.1 mm to avoid any possible singularity of stiffness matrix for the equilibrium function;

r$_{\text{max}}$ is the upper bound of the inner radius. Because of symmetry constraints applied on the micro-scale design

Table 2 Uncertainty information in material properties and loading conditions

Number	Random parameter	Symbol	Mean value	Distribution	Variation
1	Longitudinal modulus (Pa)	E_{11}	1.43×10^{11}	Normal	0.1
2	Transverse modulus (Pa)	E_{22}	1.0×10^{10}	Normal	0.1
3	In-plane shear modulus (Pa)	G_{12}	1.0×10^{9}	Normal	0.1
4	Load magnitude (N)	F	-1000	Normal	0.1
5	Direction (°)	θ	0	Normal	$10°$

variables, only half of layers are considered as design variables, and thus $j = 1, 2, ..., N^{lay}/2$.

Unlike (16), mathematical formulation of RBMDO for composite frames under uncertainties can be formulated as

$$\min_{r_i} V(r_i) = \sum_{i=1}^{N^{tub}} \pi \left[\widetilde{t_i^{tot}}^2 + 2r_i \widetilde{t_i^{tot}} \right] L_i$$

$$Subject \ to: \begin{cases} \Pr\left[G_C\left(r_i, x_{i,j,c}, R_{mat,\ \zeta}, R_{loa,\eta}\right) \le 0 \right] \le P_{fC}^{Tar} \\ S.T. K\left(D_n^e\left(r_i, x_{i,j,c}, R_{mat,\ \zeta}\right)\right) U = F\left(R_{loa,\eta}\right) \\ r_i \in [r_{min}, r_{max}] \\ x_{i,j,c} \in [0, 1] \\ i = 1, 2, ..., N^{tub}, j = 1, 2, ..., \frac{N^{lay}}{2}, c = 1, 2, ..., N^{can} \\ \zeta = 1, 2, ..., N^{R_{mat}}, \eta = 1, 2, ..., N^{R_{loa}} \\ \text{Manufacturing Constraints } (MC1 - MC6) \end{cases} \quad (17)$$

where $G_C(r_i, x_{i, j, c}, R_{mat, \zeta}, R_{loa, \eta})$ is the limit state function of structure compliance which is expressed as $C(r_i, x_{i, j, c}, R_{mat, \zeta}, R_{loa, \eta})$-$C^{Tar}$; $R_{mat, \zeta}$ and $R_{loa, \eta}$ represent the ζ-th and η-th random parameter of material properties and loading condition, respectively; $N^{R_{mat}}$ and $N^{R_{loa}}$ are the number of random parameters for material properties and loading conditions, respectively; P_{fC}^{Tar} is the target probability of failure for the compliance constraint. For the numerical examples in Sect. 7, the same C^{Tar} is used for both DMDO and RBMDO.

Structural analysis of composite frames in (16) and (17) is performed using the modified beam finite element tool called BEam Cross Section Analysis Software (BECAS) by Duan et al. (2018, 2019a, b) to apply to composite frames combined with DMO. BECAS is an analysis tool of cross sections developed by Blasques and Lazarov (2012) for anisotropic and inhomogeneous beam sections with arbitrary geometry.

## 5 Discrete material optimization and sensitivity analysis

5.1 Fundamental DMO theory

Fundamental theory of DMO used to perform DMDO and RBMDO in (16) and (17), respectively, is briefly introduced in this section. The DMO approach is implemented in a finite element framework. Then, the element constitutive matrix per layer $Q_{i,j}^e$ can be expressed as a weighted sum of the constitutive matrices $Q_{i, j, c}$ of the candidate ply angles where the superscript e refers to "element", and the subscripts i, j, and c refer to the i-th tube, j-th layer, and c-th candidate ply angles, respectively. In general, for multi-layer laminates, interpolation scheme can be implemented layer-wise for all layers in all elements. The constitutive relationship for the j-th layer can be
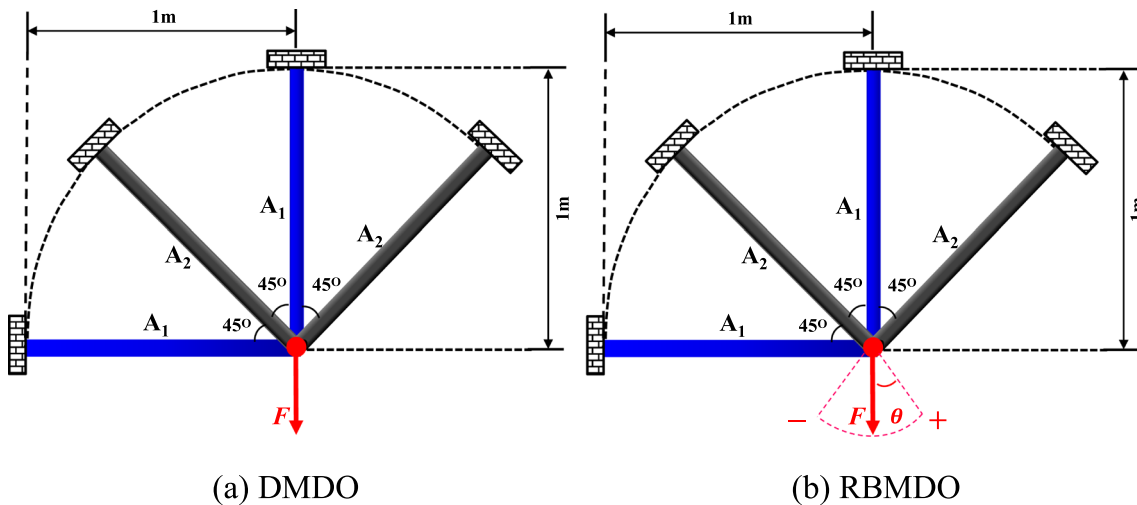
(a) DMDO   (b) RBMDO

Fig. 5 Initial configuration of 2D 4-beam composite frame for **a** DMDO with deterministic load and **b** RBMDO with uncertainties in loading magnitude and direction, $F = 10000$; + and − denote positive and negative uncertain loading direction
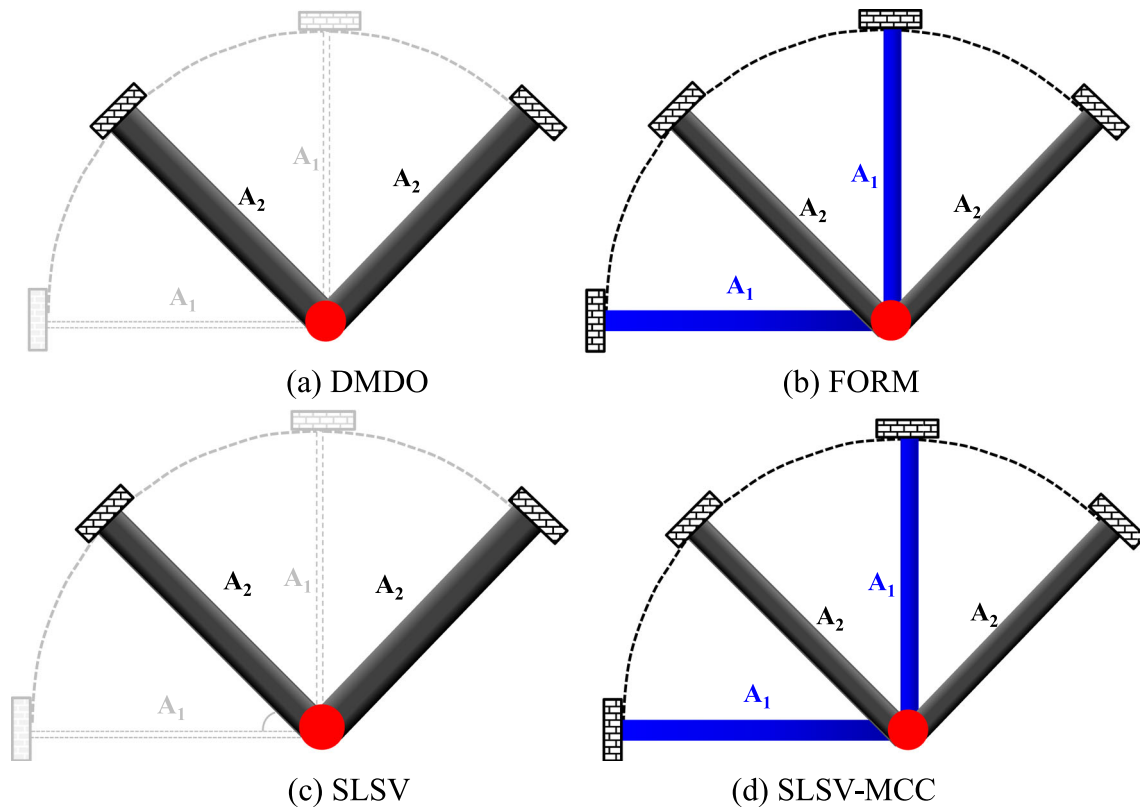
Fig. 6 Optimized topology configurations of DMDO and RBMDO for 4-beam example: **a** DMDO, **b** RBMDO with FORM, **c** RBMDO with SLSV, and **d** RBMDO with SLSV-MCC

expressed as a sum over the number of candidate ply angles N^{cand} as

$$\boldsymbol{Q}_{i,j}^e = \sum_{c=1}^{N^{cand}} \omega_{i,j,c} \boldsymbol{Q}_{i,j,c} \qquad (18)$$

where $\omega_{i,j,c}$ is the weighting function with the bound of 0 and 1 since no stiffness or mass matrix can contribute more than the physical material properties, and negative contribution is physically meaningless. Generalized solid isotropic material with penalization (SIMP) for multi-material interpolation schemes (Hvejsel and Lund 2011) is used in this paper to push the weighting function to either 0 or 1 to obtain distinct material selection. Then, the weighting function can be expressed as

$$\omega_{i,j,c} = \left(x_{i,j,c}\right)^p \qquad (19)$$

where p is the penalty parameter and $x_{i,j,c}$ is the artificial material density of candidate ply angles which satisfies

$$\sum_{c=1}^{N^{cand}} x_{i,j,c} = 1 \qquad (20)$$

5.2 Design sensitivity analysis

The global structure cost in (16) and (17) is a function of r_i only. Thus, its sensitivity with respect to r_i considering the winding layer thickness punitive strategy is given by

$$\frac{\partial V(r_i)}{\partial r_i} = 2\pi r_i \frac{t_i^{tot}}{r_i^0} \left(\frac{t_i^{tot}}{r_i^0} + 2\right) L_i \qquad (21)$$

where t_i^{tot} is the initial total thickness of the i-th tube. The manufacturing constraints in this study are formulated as a

Table 3 Comparison of optimization results obtained using DMDO and RBMDO

Method	Cost	C^{Tar}	MPP [E_{11}, E_{22}, G_{12}, F, θ]	# of FEA calls	Relative errors with MCS
DMDO	0.01278	0.12769	N.A.	233	N.A.
FORM	0.01863	0.12769	[1.3126e^{11}, 9.9988e^9, 9.9999e^9, 1.1341e^4, −4.8224]	6410	2.10%
SLSV	0.01726	0.12769	[1.3101e^{11}, 9.9940e^9, 9.9998e^9, 1.1387e^4, −2.7659]	1024	18.37%
SLSV-MCC	0.01888	0.12769	[1.3134e^{11}, 9.9995e^9, 9.9999e^9, 1.1329e^4, −5.2212]	1088	1.78%

Table 4 Optimum designs of macroscopic radii in DMDO and RBMDO

Beam number	DMDO	FORM	SLSV	SLSV-MCC
	Optimal macroscopic radii r_i, m			
A_1	r_{min}	0.01648	r_{min}	0.01657
A_2	0.06079	0.04890	0.05867	0.04977

series of linear inequalities or equalities. Thus, sensitivities of all manufacturing constraints are obtained explicitly without further derivation.

For sensitivity analysis of the structure compliance constraint, the semi-analytical method (SAM) (Cheng & Olhoff, 1993; Lund 1994; Blasques and Lazarov 2012) is adopted in this work instead of directly deriving analytical sensitivities due to its ease of derivation and implementation. SAM is computationally efficient and thus often used for sensitivity analysis of finite element models. This section only presents the compliance constraint sensitivity analysis with respect to deterministic micro-scale design variable $x_{i, j, c}$. Sensitivities of the compliance with respect to deterministic macro-scale design variable r_i can be easily obtained in a similar manner. Assume that applied static loads are design independent, then sensitivities of the structure compliance C in (16) and (17) with respect to $x_{i, j, c}$ are given as

$$\frac{\partial C}{\partial x_{i,j,c}} = \sum_{n=1}^{N^{ele}} \left(\frac{\partial U_n^T}{\partial x_{i,j,c}} K_n U_n + U_n^T \left(\frac{\partial K_n}{\partial x_{i,j,c}} U_n + K_n \frac{\partial U_n}{\partial x_{i,j,c}} \right) \right) \qquad (22)$$

where U_n is the displacement vector of element n and K_n is the corresponding element stiffness matrix. Furthermore, using

the equilibrium conditions $K_n U_n = F$, (22) can be simplified (see Bendsøe and Sigmund 2013) as

$$\frac{\partial C}{\partial x_{i,j,c}} = - \sum_{n=1}^{N^{ele}} U_n^T \frac{\partial K_n}{\partial x_{i,j,c}} U_n \qquad (23)$$

It is possible to rewrite (23) using the element stiffness matrix given by $K_n = \int_{\Omega^n} B^T D_n B \mathrm{d}\Omega^n$ where B is the strain-displacement matrix and Ω^n is the volume of the n-th finite element as

$$\frac{\partial C}{\partial x_{i,j,c}} = - \sum_{n=1}^{N^{ele}} U_n^T \int_{\Omega^n} B^T \frac{\partial D_n (x_{i,j,c}, r_i)}{\partial x_{i,j,c}} B \mathrm{d}\Omega^n \, U_n \qquad (24)$$

The SAM approach is computationally more efficient than the overall finite difference (OFD) method since factorization of the global stiffness matrix, which is the most time consuming part in the computation, is calculated once for N design variables whereas the stiffness matrix needs to be assembled and factored N + 1 times for N design variables in OFD. Then, $\frac{\partial D_n(x_{i,j,c}, r_i)}{\partial x_{i,j,c}}$ are calculated using central difference as

$$\frac{\partial D_n (x_{i,j,c}, r_i)}{\partial x_{i,j,c}} \approx \frac{D_n \left((x_{i,j,c} + \Delta x_{i,j,c}, r_i) \right) - D_n \left(x_{i,j,c} - \Delta x_{i,j,c}, r_i \right)}{2 \Delta x_{i,j,c}} \qquad (25)$$

where $\Delta x_{i, j, c}$ is a small perturbation of $x_{i, j, c}$.

The accuracy of SAM has been compared with the overall finite difference (OFD) method with a small perturbation of deterministic design variables. The sensitivities of compliance constraint with respect to deterministic design variables are not exactly obtained but the accuracy is desirable enough.

For MPP approximation in SLSV-MCC, it is necessary to perform sensitivity analysis of the compliance constraint with

Fig. 7 Iteration history of the objective function for DMDO and RBMDO
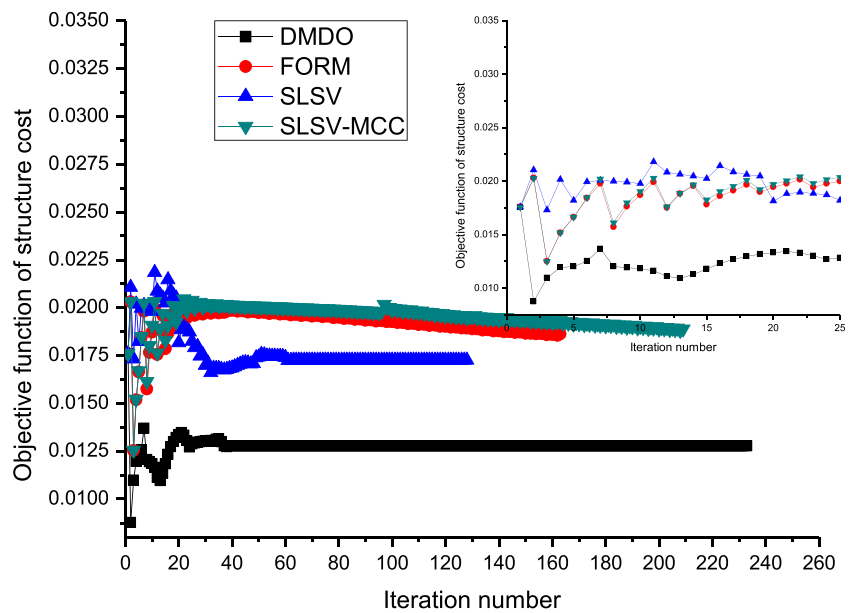
Fig. 8 Iteration history of the compliance constraint for DMDO and RBMDO
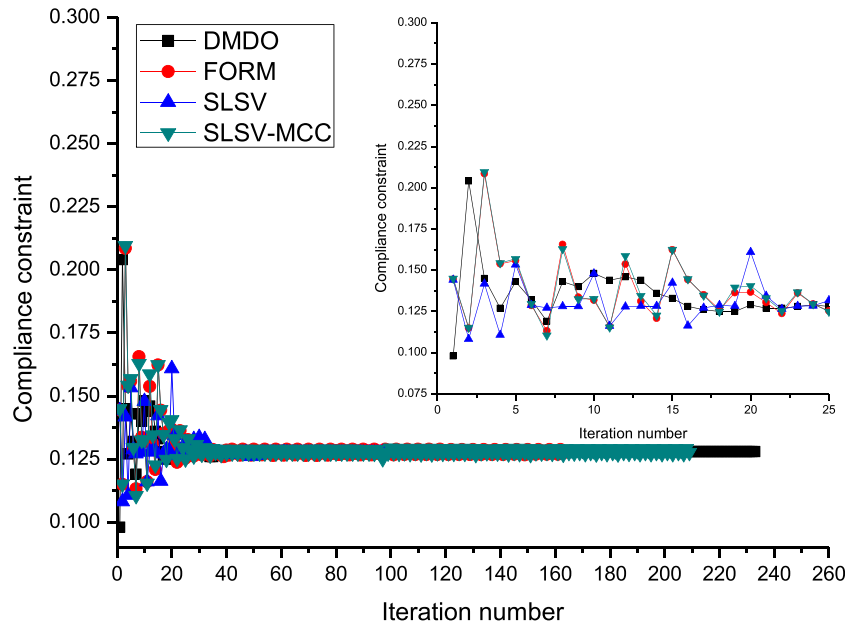
respect to random parameters ($R_{mat, \zeta}$, $R_{loa, \eta}$), i.e., $\frac{\partial C}{\partial R_{mat, \zeta}}$ and $\frac{\partial C}{\partial R_{loa,\eta}}$. In this study, they are calculated using the central difference method.

6 Typical manufacturing constraints and solution strategies

Manufacturing constraints in (16) and (17) labeled as $MC1 - MC6$ are briefly introduced in this section. Explicit linear equality and inequality equations for the manufacturing constraints are expressed in terms of $x_{i, j, c}$ in DMO. For more detailed explanation on six typical manufacturing constraints of laminated fibrous composite structures, readers can refer to Yan et al. (2017) and Duan et al. (2019a, b).

6.1 Manufacturing constraints and numerical solution steps

The first manufacturing constraint is contiguity constraint with contiguity limit of $CL \in N$ and is formulated as a linear inequality as

$$x_{i,j,c} + \cdots + x_{i,j+CL,c} \leq CL, \quad j + CL \leq N^{lay}, \quad MC1 \tag{26}$$

For any $i \in N^{tub}$, $j \in N^{lay}$, and $c \in N^{cand}$, it should follow(Imani et al., 2018), and the loop should meet the dimension of $j + CL \leq N^{lay}$. For example, if a composite tube has 20 layers, i.e., $N^{lay} = 20$, and every layer has four candidate materials, i.e., $N^{cand} = 4$, then, the total number of contiguity constraints should be calculated as $(N^{lay} - CL) \times N^{cand} = (20 - 1) \times 4 = 76$, when $CL = 1$.

The second manufacturing constraint is the 10% rule, which means that a minimum of 10% of plies of each candidate angle ($5°, \mp 45°, 85°$) is required. It is frequently adopted in engineering applications and expressed as

$$\sum_{j=1}^{N^{lay}} x_{i,j,c} \geq 0.1 N^{lay}, MC2 \tag{27}$$

The third manufacturing constraint is balance constraint, which means that angle plies (those at any angle other than $5°$ and $85°$) should occur only in balanced pairs with the same number of $+\theta°$ and $-\theta°$ plies. The parameterized linear equality constraint with respect to $x_{i, j, c}$ can be expressed as

Table 5 Optimum designs of microscopic fiber winding angles for DMDO and RBMDO

Beam Number	DMDO	FORM	SLSV	SLSV-MCC
	Optimal microscopic fiber winding angles $\theta_{i, j}$, °			
A₁	–	(85/5/5/85/5/5/-45/5/5/45)s	–	(45/5/5/85/5/5/-45/5/85/5)s
A₂	(85/5/5/85/5/5/-45/5/5/45)s	(45/5/5/85/5/5/-45/5/85/5)s	(45/5/5/-45/5/5/85/5/5/85)s	(45/5/5/85/5/5/-45/5/85/5)s

s symmetrical layers

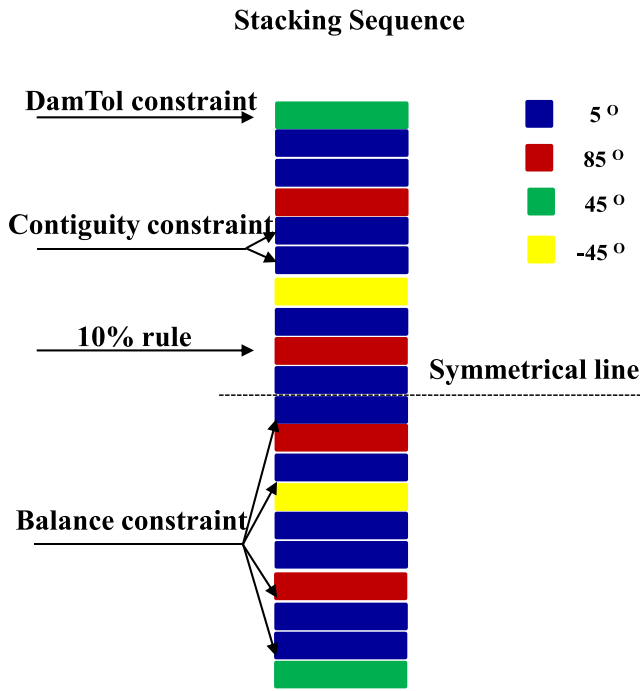"–" means that the radius reaches its lower limit r_{min}

Stacking Sequence

Fig. 9 Detailed manufacturing constraints in A_2 tubes of SLSV-MCC

$$\sum_{j=1}^{N^{\text{lay}}} x_{i,j,+c} - \sum_{j=1}^{N^{\text{lay}}} x_{i,j,-c} = 0, \quad c \neq (5° \cup 85°), \quad MC3 \qquad (28)$$

where $x_{i,j,+c}$ and $x_{i,j,-c}$ denote a positive and an accompanied negative angle, respectively.

The fourth manufacturing constraint is damage tolerance constraint, which means that 5° ply along the axial direction cannot be selected in the inner and outer layers. This constraint can be expressed as the artificial density of 5° candidate material in the outer surface which is set to be zero, and the same as in the inner surface, i.e., $x_{i,1,c} = 0; x_{i,N^{\text{lay}},c} = 0, \; (c \in [5°])$, which are combined into one equality constraint as

$$x_{i,1,c} + x_{i,N^{\text{lay}},c} = 0, c \in [5°], \quad MC4 \qquad (29)$$

As an alternative strategy, $MC4$ constraint can be also realized through the micro-scale DMO material interpolation strategy which means that the candidate material set of the outer and inner surfaces does not contain 5° candidate material.

The fifth manufacturing constraint is symmetry constraint, which means that the fiber winding sequence should be symmetric with respect to the mid-plane. In the case of the composite tube in this study, the mid-plane specifically refers to the average radius plane of the tube. Then, the symmetry constraint can be formulated as a linear equality as

$$x_{i,j,c} = x_{i,N^{\text{lay}}-j+1,c}, \quad MC5 \qquad (30)$$

The sixth manufacturing constraint ($MC6$) is the normalization constraint in (20) to keep physical meaning in the case of a volume constraint or eigenfrequency optimization.

A flowchart for numerical implementation of RBMDO with SLSV-MCC in design optimization of composite frames in this paper is shown in Fig. 4. The detailed process of SLSV-MCC to approximate the MPP can be referred to Fig. 2b.

6.2 Solution strategies

6.2.1 Continuation strategy

In order to obtain discrete designs in the micro-scale, a continuation strategy for the penalization parameter p in (19) is adopted in this paper. The initial penalty parameter p is set to be 1. It has been shown by Hvejsel and Lund (2011) that p larger than 3 will not help too much to penalize intermediate values of design variables. Hence, p linearly increases in this study with slope of 0.5 in every ten iterations from 1 to 3.

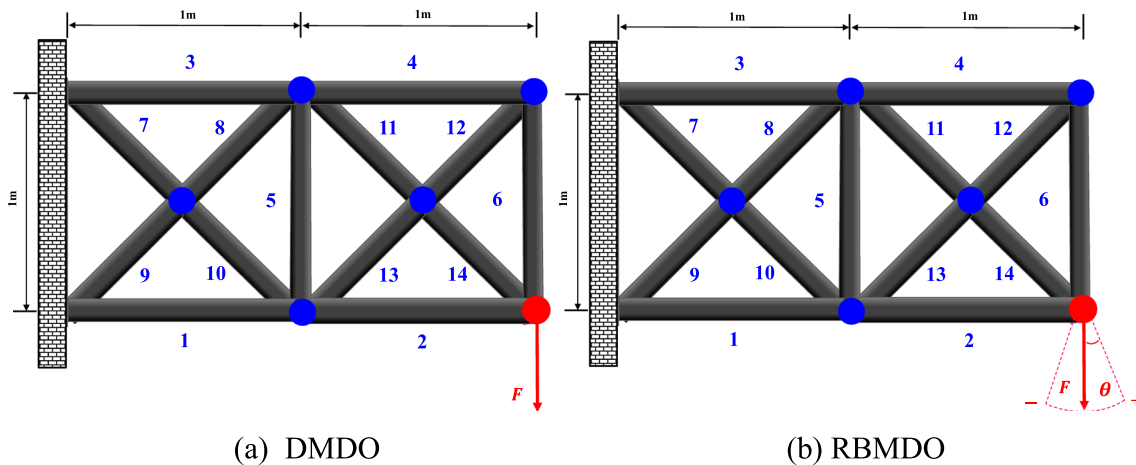(a) DMDO   (b) RBMDO

Fig. 10 Initial configuration of 2D 14-beam composite frame for **a** DMDO with deterministic load. **b** RBMDO with uncertainties in loading magnitude and direction, $F = 10000$

Table 6 Comparison of optimization results obtained using DMDO and RBMDO

Method	Cost	C^{Tar}	MPP [E_{11}, E_{22}, G_{12}, F, θ]	# of FEA calls	Relative errors with MCS
DMDO	0.01801	4.16679	N.A.	106	N.A.
FORM	0.02402	4.16679	[$1.3141e^{11}$, $9.9850e^9$, $9.9997e^9$, $1.1365e^4$, 4.2850]	9280	2.15%
SLSV	0.02366	4.16679	[$1.3150e^{11}$, $9.9840e^9$, $9.9997e^9$, $1.1361e^4$, 4.1372]	1096	4.35%
SLSV-MCC	0.02389	4.16679	[$1.3148e^{11}$, $9.9828e^9$, $9.9997e^9$, $1.1364e^4$, 4.4309]	808	3.25%

6.2.2 Winding layer thickness punitive strategy

To realize topology optimization in the macro-structural scale and reduce the number of design variables, a linear punitive relationship between micro winding layer thickness and macro-scale tube radius is adopted as

$$\widetilde{t}_i = \frac{r_i}{r_0} \times t_0, i \in N^{Tub} \; if \, r_i < r_0 \qquad (31)$$

where $\widetilde{t}_i$ is the single layer thickness of the i-th tube after punishment, t_0 is the initial layer thickness, and r_0 is the initial inner radius of the tube. In (31), the layer thickness will change as the inner radius changes when $r_i < r_0$. Otherwise, the layer thickness will be kept as t_0. Based on the ground structure approach of topology optimization, small r_i means that the tube has lower contribution to stiffness of the whole structure, so that more material can be allocated in other tubes to improve the stiffness. For more discussion on this strategy, readers can refer to Duan et al. (2018, 2019a, b).

7 Numerical examples and discussions

In this section, two 2D and one 3D numerical examples are investigated to validate effectiveness of the proposed RBMDO with SLSV-MCC in design optimization of composite frames. In three numerical examples, DMDO and RBMDO with FORM and SLSV are performed as well for comparison. MCS is utilized to validate accuracy of these methods in two 2D examples.

The specific manufacturing constraints are considered in both DMDO and RBMDO. Considering practical engineering

(a) DMDO

(b) FOR

(c) SLSV
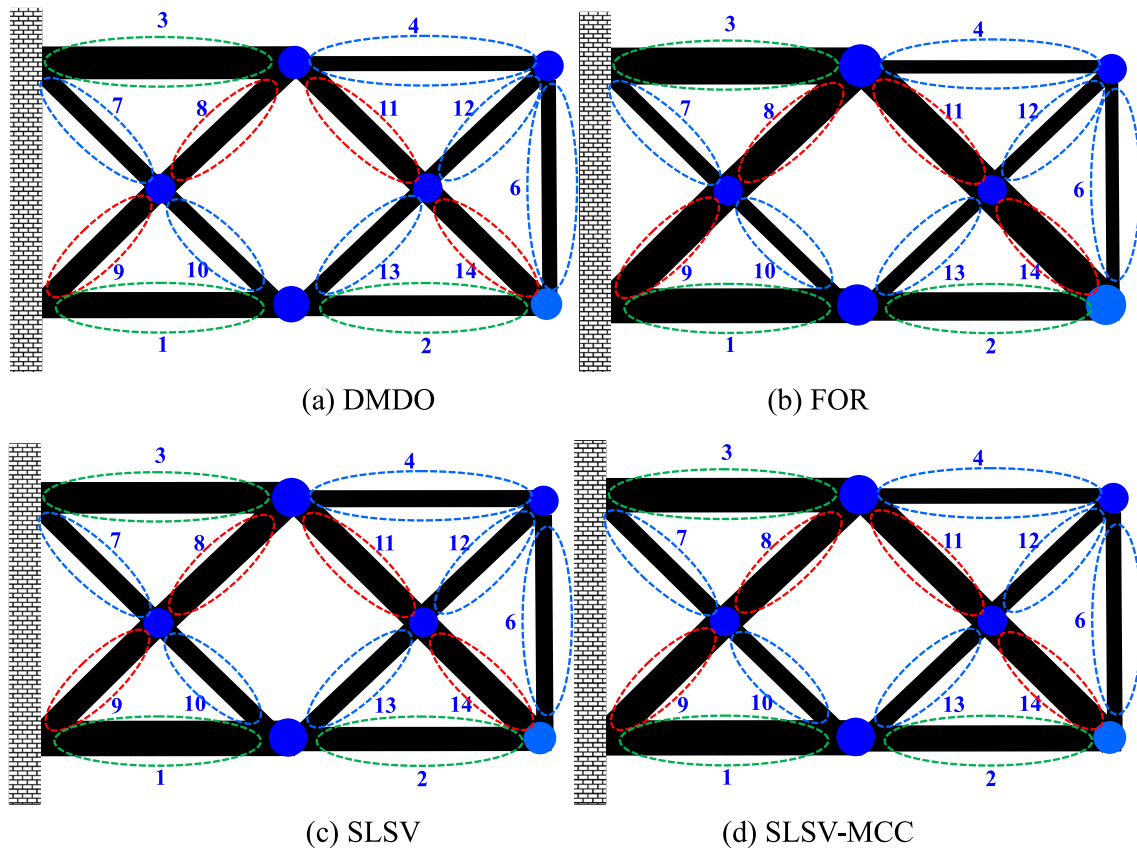
(d) SLSV-MCC

Fig. 11 Optimized topology configurations of DMDO and RBMDO for 14-beam example: **a** DMDO, **b** RBMDO with FORM, **c** RBMDO with SLSV, **d** RBMDO with SLSV-MCC

**Table 7** Optimum designs of macroscopic radii in DMDO and RBMDO

Beam number	DMDO	FORM	SLSV	SLSV-MCC
	Optimal macroscopic radii r_i, m			
1	0.01897	0.02564	0.02603	0.02558
2	0.01513	0.02085	0.01782	0.01898
3	0.02386	0.02716	0.02316	0.02510
4	0.01099	0.00977	0.01254	0.01132
5	r_{min}	r_{min}	r_{min}	r_{min}
6	0.01104	0.00979	0.01258	0.01134
7	0.01275	0.01143	0.01448	0.01318
8	0.01677	0.02474	0.02106	0.02171
9	0.01691	0.02552	0.01941	0.02246
10	0.01265	0.01141	0.01441	0.01309
11	0.01715	0.02639	0.01983	0.02220
12	0.01262	0.01141	0.01434	0.01287
13	0.01274	0.01143	0.01448	0.01316
14	0.01725	0.02761	0.02046	0.02217

applications, it is assumed that each composite tube has the same number of layers, i.e., $N^{lay} = 20$, and the 20 layers have identical thickness of 0.1 mm in the initial design, i.e., $t_i^{tot}/N^{lay} = 0.1$ mm. The initial value of the inner radius is $r_{init} = 25$ mm, and the upper and lower limits are $r_{max} = 75$ mm and $r_{min} = 0.1$ mm, respectively. The contiguity limit CL is set as CL = 2. The fiber candidate materials are carbon fiber-reinforced epoxy (CFRE) with orthotropic properties as shown in Table 1. Table 2 lists uncertainty information of three composite material properties, E_{11}, E_{22}, and G_{12}, and two loading conditions, magnitude and direction.

In three numerical examples, the target probability of failure is set as $P_{fC}^{Tar} = 5\%$. The number of finite element analysis (FEA) evaluations is used as a measure of efficiency. MCS with 10^5 samples is performed considering computational costs in engineering problems. In all methods, the same initial design variables and convergence criteria are used. Considering all the manufacturing constraints explained in Sect. 6.1, the number of design variables in each tube is 40 which contains 1 sizing design variable (r_i) and 39 candidate material density design variables ($x_{i, j, c}$). It should be noted that $x_{i, j, c} = \left(\frac{N^{lay}}{2}\right) \times N^{cand} = 10 \times 4 = 40$ from the symmetry constraint, and the damage tolerance constraint ($MC4$) is realized through the micro-scale DMO material interpolation strategy. Thus, the actual number of $x_{i, j, c}$ becomes 39.

There are seven types of constraints: one reliability compliance constraint related with random parameters and six manufacturing constraints that are independent of random parameters. The symmetry constraint ($MC5$) and damage tolerance constraint ($MC4$) are realized by design variable linking and DMO material interpolation without 5° candidate material, respectively. Hence, there are total 47 manufacturing constraints in each tube: 32 contiguity constraints ($MC1$) since CL = 2, 4 10% rule constraints ($MC2$), 10 DMO normalization constraints ($MC6$), and 1 balance constraint ($MC3$). With the first 2D 4-beam composite frame as example, the total number of manufacturing constraints is 94. The detailed convergent results are presented in form of fiber winding angles and schematic diagram as in Fig. 7.

Fig. 12 Iteration history of the objective function for DMDO and RBMDO
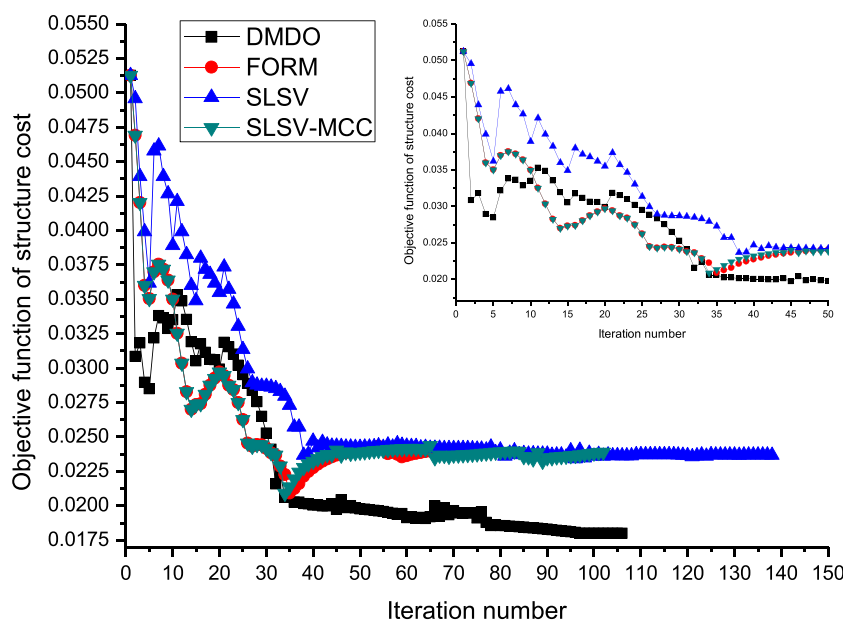
Fig. 13 Iteration history of the compliance constraint for DMDO and RBMDO
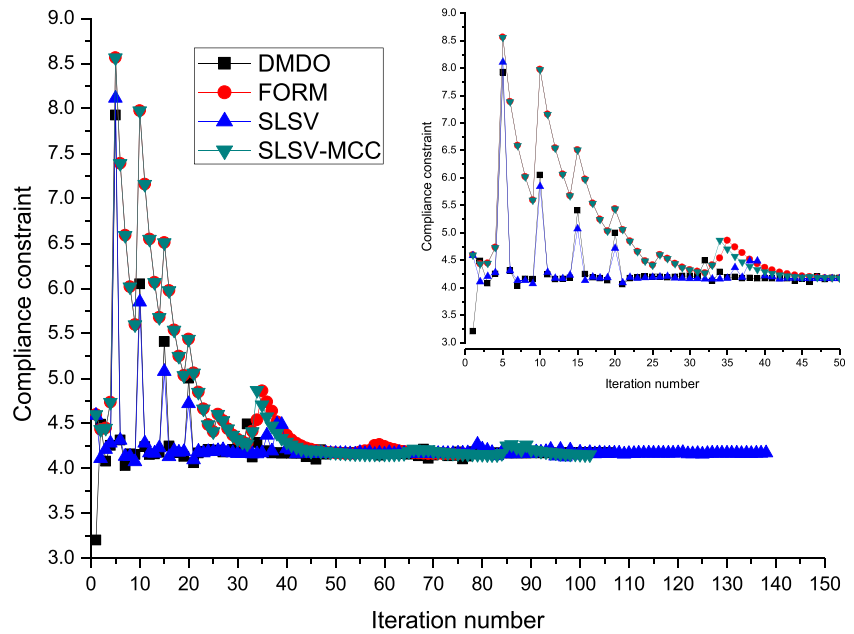
7.1 2D 4-beam composite frame

For the first example, a simple 2D 4-beam composite frame is introduced for RBMDO. Its initial geometric sizes, loading, and bounndary conditions for DMDO and RBMDO are shown in Fig. 5a and b. Four tubes are divided into two groups as labeled A_1 and A_2 in different colors. The total numbers of deterministic design variables, manufacturing constraints, compliance constraints, and random parameters are 80, 94, 1, and 5, respectively. The initial structural cost is V = 0.01759.

For RBMDO, three reliability analysis methods—FORM, SLSV, and SLSV-MCC—are utilized for comparison. Table 5 presents detailed optimization results of DMDO and RBMDO with three methods, and optimized topology configurations of DMDO and RBMDO are shown in Fig. 6. From Table 3 and Fig. 6, four observations can be made:

(1) The proposed SLSV-MCC shows much better efficiency and accuracy than FORM (6410 vs 1088) and SLSV (18.37% vs 1.78%).

Table 8 Optimum designs of microscopic fiber winding angles for DMDO and RBMDO

Beam number	DMDO	FORM	SLSV	SLSV-MCC
	Optimal microscopic fiber winding angles $\theta_{i,\,j}$, °			
1	(45/5/5/85/5/-45/5/85/5/5)s	(45/5/5/85/5/-45/5/85/5/5)s	(45/5/5/85/-45/5/5/85/5/5)s	(45/5/5/85/5/-45/5/85/5/5)s
2	(45/5/5/85/5/-45/5/85/5/5)s	(45/5/5/85/5/-45/5/85/5/5)s	(45/5/5/85/-45/5/5/85/5/5)s	(45/5/5/85/5/-45/5/85/5/5)s
3	(45/5/5/85/5/-45/5/85/5/5)s	(45/5/5/85/5/-45/5/85/5/5)s	(45/5/5/85/5/5/-45/85/5/5)s	(45/5/5/-45/5/85/5/85/5/5)s
4	(45/5/5/85/5/-45/5/85/5/5)s	(45/5/5/85/5/-45/5/85/5/5)s	(45/5/5/85/5/85/5/5/-45/5)s	(45/5/5/85/5/5/-45/85/5/5)s
5	–	–	–	–
6	(45/5/5/85/5/-45/5/85/5/5)s	(45/5/5/85/5/-45/5/85/5/5)s	(45/5/5/85/5/85/5/5/-45/5)s	(45/5/5/85/5/-45/5/85/5/5)s
7	(45/5/5/85/5/-45/5/85/5/5)s	(45/5/5/85/5/-45/5/85/5/5)s	(45/5/5/85/5/85/5/5/-45/5)s	(45/5/5/85/5/5/-45/85/5/5)s
8	(45/5/5/85/5/5/-45/85/5/5)s	(45/5/5/85/5/85/5/5/-45/5)s	(45/5/5/85/5/85/5/-45/5)s	(45/5/5/85/5/-45/5/85/5/5)s
9	(45/5/5/85/5/5/-45/85/5/5)s	(45/5/5/85/5/85/5/5/-45/5)s	(45/5/5/85/5/5/-45/85/5/5)s	(45/5/5/85/5/-45/5/85/5/5)s
10	(45/5/5/85/5/-45/5/85/5/5)s	(45/5/5/85/5/-45/5/85/5/5)s	(45/5/5/85/5/85/5/5/-45/5)s	(45/5/5/85/5/5/-45/85/5/5)s
11	(45/5/5/85/5/5/-45/85/5/5)s	(45/5/5/85/5/85/5/5/-45/5)s	(45/5/5/85/5/-45/5/85/5/5)s	(45/5/5/85/5/-45/5/85/5/5)s
12	(45/5/5/85/5/-45/5/85/5/5)s	(45/5/5/85/5/-45/5/85/5/5)s	(45/5/5/85/5/85/5/5/-45/5)s	(45/5/5/85/5/5/-45/85/5/5)s
13	(45/5/5/85/5/-45/5/85/5/5)s	(45/5/5/85/5/-45/5/85/5/5)s	(45/5/5/85/5/85/5/5/-45/5)s	(45/5/5/85/5/-45/5/85/5/5)s
14	(45/5/5/85/5/5/-45/85/5/5)s	(45/5/5/85/5/85/5/5/-45/5)s	(45/5/5/85/5/-45/5/85/5/5)s	(45/5/5/85/5/-45/5/85/5/5)s

s symmetrical layers

"–" means that the radius reaches its lower limit r_{min}
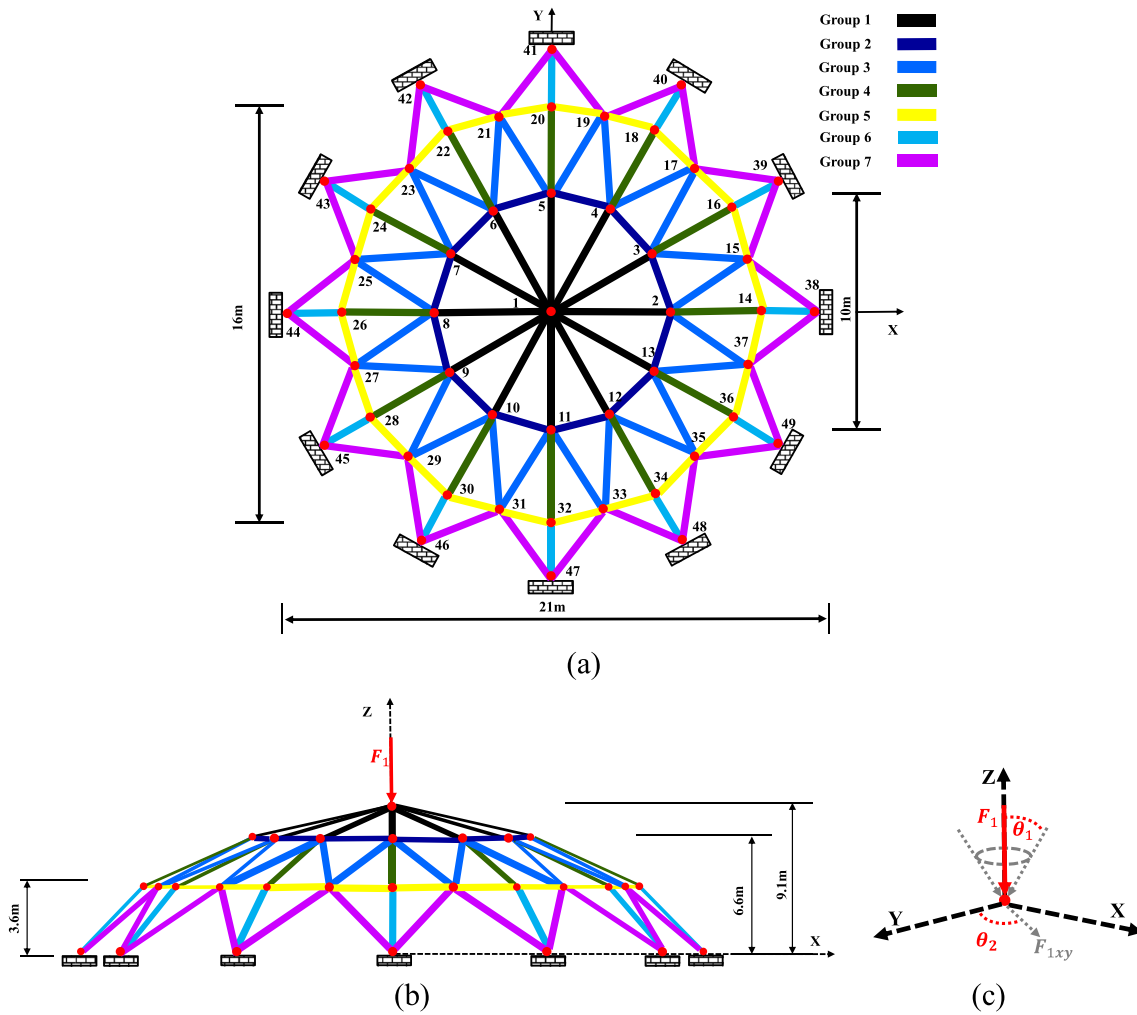
Fig. 14 Initial configuration of spatial 120-beam composite frame for DMDO and RBMDO: **a** the top view of 120-beam composite frame, **b** the side view of 120-beam composite frame for DMDO with deterministic load, and **c** uncertainty in loading magnitude and directions (θ_1, θ_2), $F_1 = 10{,}000$

(2) The proposed SLSV-MCC shows similar efficiency and accuracy as SLSV (1024 vs 1088) and FORM (2.10% vs 1.78%).

(3) Figure 6 shows that the optimized topology configurations can be categorized into two types: 2-beam structure in DMDO and SLSV and 4-beam structure in FORM and SLSV-MCC. The detailed values of r_i in all the optimum designs are presented in Table 4.

(4) MPPs for loading direction in FORM and SLSV-MCC (− 4.8224° and − 5.2212°) show that horizontal loading is considered in RBMDO with FORM and SLSV-MCC yielding 4-beam optimal structure with thicker A_2 tubes

and thinner A_1 tubes. On the other hand, SLSV with relatively small MPP value in loading direction (− 2.7659°) and DMDO with no consideration of horizontal loading yield 2-beam optimal structure where A_1 tubes reached the lower limit and thus are eliminated.

Iteration histories of the cost and compliance constraint for DMDO and RBMDO are presented in Figs. 7 and 8 where histories of the initial 25 iterations are shown for clearer demonstration. In Fig. 8, compliance constraints of RBMDO are evaluated at MPP. As observed in the figures, RBMDO

Table 9 Comparison of optimization results between DMDO and RBMDO with SLSV-MCC

Method	Cost	C^{Tar}	MPP [E_{11}, E_{22}, G_{12}, F, θ_1, θ_2]	# of FEA calls	Relative errors with MCS
DMDO	1.30182	0.91380	N.A.	115	N.A.
SLSV-MCC	1.55196	0.91380	[1.3134e^{11}, 9.9999e^9, 9.9999e^9, 1.1328e^4, 5.2671, 0.0379]	1528	2.36%
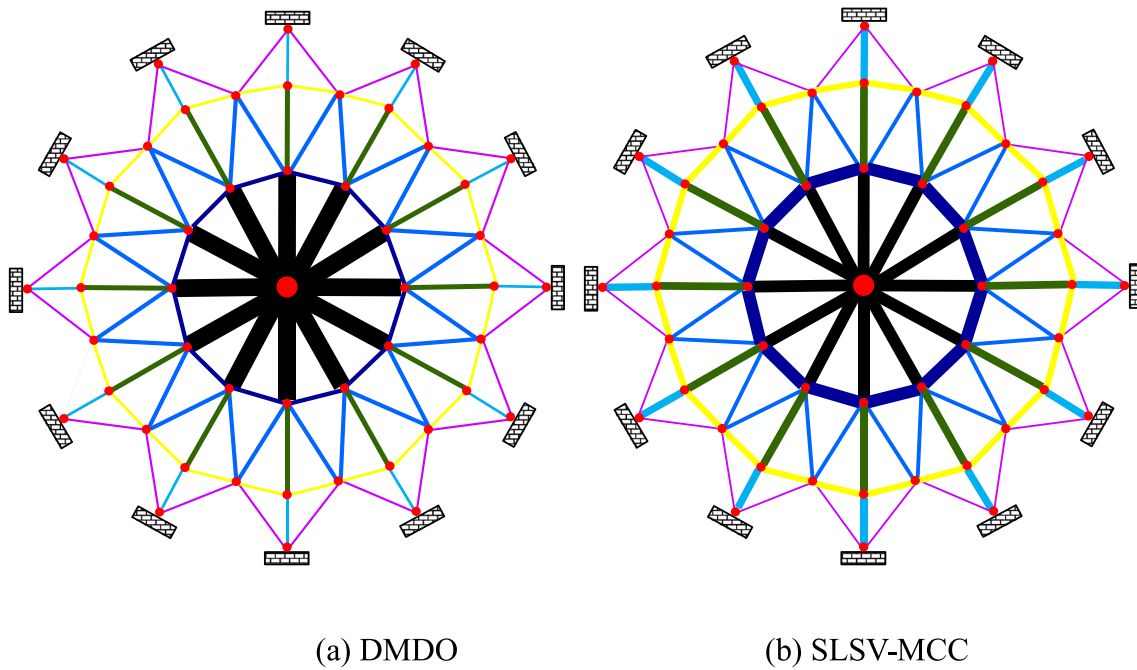
(a) DMDO   (b) SLSV-MCC

Fig. 15 Optimized topology configurations of DMDO and RBMDO with SLSV-MCC for 120-beam example: **a** DMDO and **b** RBMDO with SLSV-MCC

utilizes more structure cost to satisfy the compliance constraint with $P_{fC}^{Tar} = 5\%$. The objective function of DMDO is reduced by 27.29% from the initial cost V = 0.01759, but the DMDO optimum will have higher risk of failure under uncertainties of material properties and loading conditions. All the optimum designs of DMDO and RBMDO well converged strictly satisfying the compliance constraint.

Detailed optimal results of $\theta_{i, j}$ are presented in Table 5 which shows that all the micro-scale fiber winding angles strictly follow the specific manufacturing constraints. Figure 9 shows detailed manufacturing constraints on micro-scale design variables using A$_2$ tubes of SLSV-MCC. Because the outer and inner layers cannot contain 5° candidate material, there is no 5° ply placed in the outer layer of the laminate. Since CL = 2, more 5° candidate fiber winding angles are

selected because they are beneficial to improve axial stiffness of the structure. However, larger CL may lead to crack propagation in the laminate ultimately. So in most engineering applications, CL is set between 2 and 3, especially in aerospace engineering. Without the 10% rule constraint, 85° fiber winding angles may not appear. The 10% rule effectively avoids a single fiber angle to dominate excessively to make the laminate more robust in the sense that they are less susceptible to weaknesses associated with highly orthotropic laminates.

7.2 2D 14-beam composite frame

To further verify capability of the proposed SLSV-MCC, a 2D 14-beam composite frame is investigated. Its initial geometric

Table 10 Optimum designs of DMDO and RBMDO with SLSV-MCC

Beam number	DMDO		SLSV-MCC	
	r_i, m	$\theta_{i, j}$, °	r_i, m	$\theta_{i, j}$, °
Group 1	0.07456	(45/5/5/85/5/-45/5/85/5/5)s	0.04919	(45/5/5/85/5/-45/5/85/5/5)s
Group 2	0.01768	(45/5/5/85/5/-45/5/85/5/5)s	0.05152	(45/5/5/85/5/85/5/5/-45/5)s
Group 3	0.01750	(45/5/5/85/5/85/5/5/-45/5)s	0.01587	(45/5/5/85/5/-45/5/85/5/5)s
Group 4	0.02077	(45/5/5/85/5/-45/5/85/5/5)s	0.03226	(45/5/5/85/5/-45/5/85/5/5)s
Group 5	0.01207	(45/5/5/85/5/-45/5/85/5/5)s	0.02576	(45/5/5/85/5/85/5/5/-45/5)s
Group 6	0.01116	(45/5/5/85/5/85/5/5/-45/5)s	0.03045	(45/5/5/85/5/-45/5/85/5/5)s
Group 7	0.00876	(45/5/5/85/5/-45/5/85/5/5)s	0.00790	(45/5/5/85/5/-45/5/85/5/5)s

s symmetrical layers

"–" means that the radius reaches its lower limit r$_{min}$
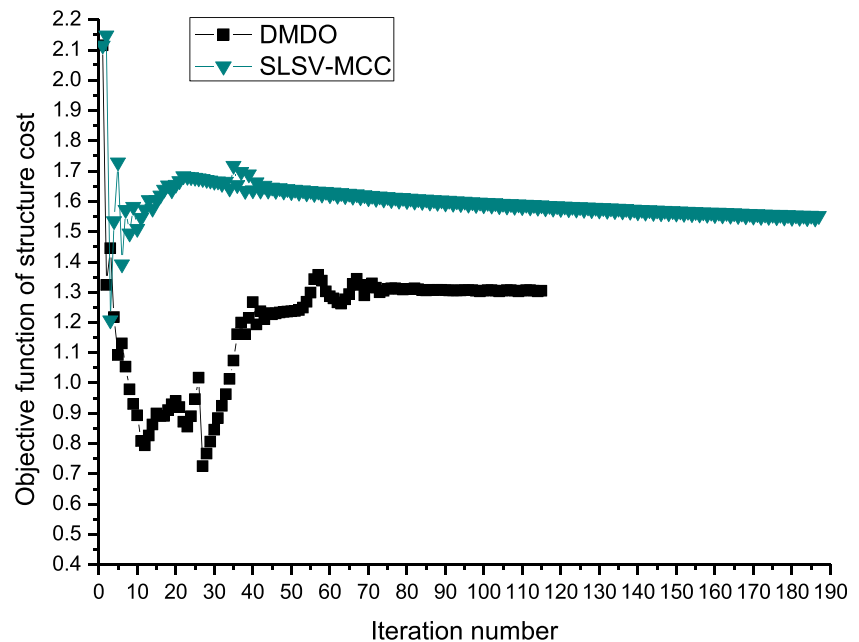
sizes, loading, and bounndary conditions for DMDO and RBMDO are shown in Fig. 10a and b, respectively. The total numbers of deterministic design variables, manufacturing constraints, compliance constraints, and random parameters are 560, 658, 1, and 5, respectively, with the initial structure cost of V = 0.05127.

Table 6 presents detailed optimization results of DMDO and RBMDO with three methods, and optimized topology configurations of DMDO and RBMDO are shown in Fig. 11. For convenience of discussion, the optimized tubes are divided into three groups which are labeled with dashed line

in green (1st-3rd tubes), blue (4th, 6th, 7th, 10th, 12nd, 13rd tubes), and red (8th, 9th, 11th, 14th tubes), respectively.

Similarly with Example 1,

(1) FEA calls of SLSV-MCC is 808, which is much less than FORM (# of FEA calls = 9280) with saving the computational cost about 91.28% while maintaining its accuracy since the relative error compared with MCS is 2.15%.

(2) Compared with SLSV, SLSV-MCC is more accurate and even more efficient since it has less number of design iterations.
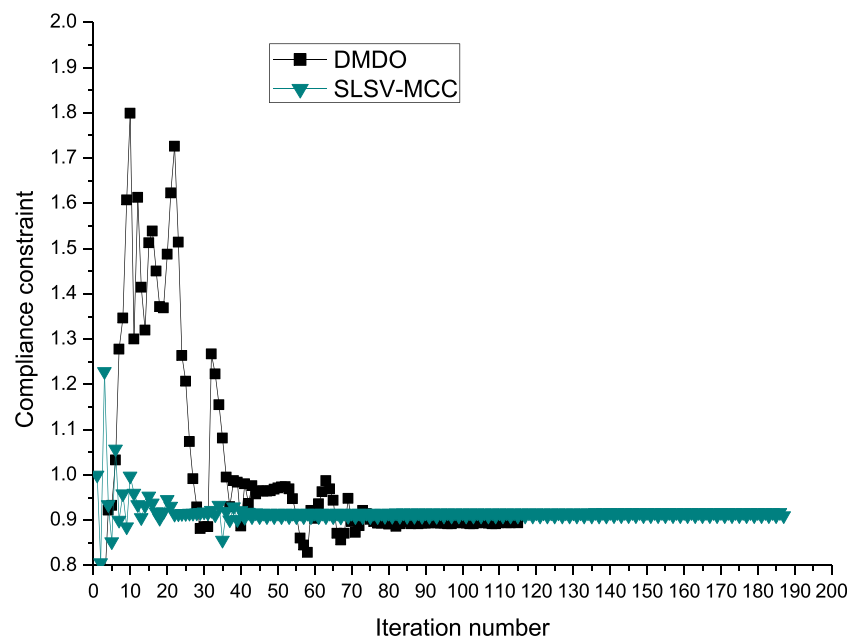
(3) Figure 11 shows that the optimized topology configurations are identical for DMDO and RBMDO. However, their optimal designs are quite different as can be seen from Table 7. The 5th tube has reached the lower limit for all the approaches. To satisfy the reliability constraint, the optimized radii of RBMDO are thicker than those of DMDO.

Iteration histories of the cost and compliance constraint for DMDO and RBMDO are presented in Figs. 12 and 13 where histories of the initial 50 iterations are shown for clearer demonstration. From Figs. 12 and 13 and Table 6, it can be seen that DMDO, FORM, SLSV, and SLSV-MCC reduced the structural cost by 64.87%, 53.15%, 53.85%, and 53.40%, respectively. Figure 13 also shows that all the optimum designs of DMDO and RBMDO well converged while strictly satisfying the compliance constraint. Detailed optimal results of $\theta_{i,j}$ are presented in Table 8 which shows that all the micro-scale fiber winding angles strictly follow the specific manufacturing constraints. It should be pointed out that combination of winding sequences is limited due to the layer number limit and contiguity limit.

7.3 Spatial 120-beam composite frame

Multi-scale design optimization of a spatial 120-beam composite is introduced for the last example. Its boundary conditions and geometric sizes are modeled according to Huu et al. (2018) and are categorized into seven groups in different colors as shown in Fig. 14. The total number of deterministic design variables, manufacturing constraints, and compliance constraints are 280, 329, and 1, respectively, with the initial structure cost of V = 2.11494. The number of random parameters is 6: 3 random material properties, 1 loading magnitude, and 2 loading directions. In this example, comparison between DMDO and SLSV-MCC is performed.

Detailed optimization results and configurations of DMDO and RBMDO with SLSV-MCC are shown in Table 9 and Fig. 15, respectively. Table 9 shows that very accurate optimization result is obtained using RBMDO with SLSV-MCC, and MPP value of θ_1 is much larger than that of θ_2. This is reasonable because the structure is rotationally symmetrical, and thus, uncertainty of θ_2 will not affect the structural failure significantly. Optimal designs of DMDO and RBDMO with SLSV-MCC are presented in Table 10. The structural cost of SLSV-MCC is about 19.21% higher than that of DMDO. The optimal radii of group 1 for DMDO are much larger than those from SLSV-MCC and other groups. The optimal structures use more material in group 2 and group 5 in ring-in direction and group 4 and group 6 in radial direction.

Iteration histories of the cost and compliance constraint for DMDO and RBMDO with SLSV-MCC are presented in Figs. 16 and 17. As observed in Fig. 16 and Table 9, the optimized structural cost of DMDO and SLSV-MCC are reduced by 38.48% and 26.62%, respectively. Figures also show that both DMDO and SLSV-MCC are well converged and strictly follow the compliance constraint.

8 Conclusion

This paper proposes an efficient reliability analysis methodology, SLSV-MCC, to realize RBMDO of composite frames with considering uncertainties of material properties and loading conditions. Efficiency and accuracy of SLSV-MCC are compared with FORM and SLSV approaches, and the MCS method is utilized to validate accuracy of these approaches. Planar and spatial numerical examples show effectiveness of the proposed SLSV-MCC for structural optimization to minimizing the cost and subjecting to compliance constraint compared with FORM and SLSV. It is shown from the numerical examples that the optimized structure configurations between DMDO and RBMDO are indeed different. It is also shown that specific manufacturing constraints are strictly kept in all the numerical examples.

Compliance with ethical standards

Conflict of interest The authors declare that they have no conflict of interest.

Replication of results The raw/processed data required to reproduce these findings will be made available upon request by contact with the corresponding authors.

Appendix A: Evaluation of convergence

The convergence measure given in Stegmann and Lund (2005) is adopted to describe whether the optimization has converged to a satisfactory result, i.e., a single candidate material has been chosen in a specified element and all other materials have been discarded. For each layer, the following inequality is evaluated as

$$\omega_{i,j,c} \geq \varepsilon \sqrt{\omega_{i,j,1}^2 + \omega_{i,j,2}^2 + \cdots + \omega_{i,j,\mathrm{N}^{\mathrm{cand}}}^2} \qquad (A-1)$$

where ε is the tolerance, typically, $\varepsilon \in [0.95{\sim}0.99]$. If the

inequality in (A-1) is satisfied for any $\omega_{i, j, c}$ in the j-th layer, then the layer is flagged as converged. The convergence assessment criterion H_ε is defined as the ratio between the number of converged layers $N_c^{l,tot}$ and the total number of layers $N^{l, tot}$. N^{lay} is the number of layers in each tube, and it is assumed that each tube has the same number of layers in the paper. N^{tub} is the number of tubes in the frame structure. Thus, $N^{l, tot}$ can be expressed as the number of tubes multiplied by the number of layers in a tube, that is, $N^{l, tot} = N^{tub} \cdot N^{lay}$. Then, the convergence assessment H_ε can be expressed as

$$H_\varepsilon = \frac{N_c^{l,tot}}{N^{l,tot}} \qquad (A-2)$$

If the tolerance is 0.95 and the optimization is fully converged, i.e., $H_{\varepsilon = 0.95} = 1$, all layers have a single weight factor that contributes more than 95% to the Euclidian norm of the weight factors. More discussion about convergence criteria can be found in the references (Xu et al. 2019; Duan et al. 2015).

References

Andreasen CS, Sigmund O (2012) Multiscale modeling and topology optimization of poroelastic actuators. Smart Mater Struct 21(6):065–005

António CC, Hoffbauer LN (2009) An approach for reliability-based robust design optimisation of angle-ply composites. Compos Struct 90(1):53–59

Bailie JA, Ley RP, Pasricha A (1997) A summary and review of composite laminate design guidelines, technical report NASA, NAS1–19347, Northrop Grumman-military aircraft systems division, Final 22

Bendsøe MP, Sigmund O (2013) Topology optimization: theory, methods, and applications. Springer Science & Business Media

Blasques JP, Lazarov B (2012) User's Manual for BECAS: A cross section analysis tool for anisotropic and inhomogeneous beam sections of arbitrary geometry. Risø DTU–National Laboratory for Sustainable Energy

Chen X, Hasselman T, Neill D (1997) Reliability based structural design optimization for practical applications, 38th Structures, structural dynamics, and materials conference., 1403

Chiralaksanakul A, Mahadevan S (2005) First-order approximation methods in reliability-based design optimization. J Mech Des 127(5):851–857

Coelho PG, Fernandes PR, Guedes JM, Rodrigues HC (2008) A hierarchical model for concurrent material and topology optimisation of three-dimensional structures. Struct Multidiscip Optim 35(2):107–115

Cheng GD, Olhoff N (1993) Rigid body motion test against error in semianalytical sensitivity analysis. Comput Struct 46(3):515–527

Cho HY, Choi KK, Gaul NJ, Lee IJ, Lamb D, Gorsich D (2016) Conservative reliability-based design optimization method with insufficient input data. Struct Multidiscip Optim 54(6):1609–1630

Deng JD, Chen W (2017) Concurrent topology optimization of multiscale structures with multiple porous materials under random field loading uncertainty. Struct Multidiscip Optim 56(1):1–19

Deng JD, Yan J, Cheng GD (2013) Multi-objective concurrent topology optimization of thermoelastic structures composed of homogeneous porous material. Struct Multidiscip Optim 47(4):583–597

Denny M (2001) Introduction to importance sampling in rare-event simulations. Eur J Phys 22(4):403

Kiureghian AD, Lin HZ, Hwang SJ (1987) Second-order reliability approximations. J Eng Mech 113(8):1208–1225

Keshtegar B, Hao P, Meng Z (2017) A self-adaptive modified chaos control method for reliability-based design optimization. Struct Multidiscip Optim 55(1):63–75

Duan ZY, Yan J, Zhao GZ (2015) Integrated optimization of the material and structure of composites based on the Heaviside penalization of discrete material model. Struct Multidiscip Optim 51(3):721–732

Duan ZY, Yan J, Lee IJ, Wang JY, Yu T (2018) Integrated design optimization of composite frames and materials for maximum fundamental frequency with continuous fiber winding angles. Acta Mech Sinica 34(6):1084–1094

Duan ZY, Yan J, Lee IJ, Lund E, Wang JY (2019a) A two-step optimization scheme based on equivalent stiffness parameters for forcing convexity of Fiber winding angle in composite frames. Struct Multidiscip Optim 59(6):2111–2129

Ferreira RTL, Rodrigues HC, Guedes JM, Hernandes JA (2013) Hierarchical optimization of laminated fiber reinforced composites. Compos Struct 107:246–259

Foldager J, Hansen JS, Olhoff N (1998) A general approach forcing convexity of ply angle optimization in composite laminates. Struct Optim 16(2–3):201–211

Gao T, Zhang WH, Duysinx P (2013) Simultaneous design of structural layout and discrete fiber orientation using bi-value coding parameterization and volume constraint. Struct Multidiscip Optim 48(6):1075–1088

Guo X, Bai W, Zhang W, Gao X (2009) Confidence structural robust design and optimization under stiffness and load uncertainties. Comput Methods Appl Mech Eng 198(41–44):3378–3399

Guo X, Zhao X, Zhang W, Yan J, Sun G (2015) Multi-scale robust design and optimization considering load uncertainties. Comput Methods Appl Mech Eng 283:994–1009

Helton JC, Davis FJ (2003) Latin hypercube sampling and the propagation of uncertainty in analyses of complex systems. Reliab Eng Syst Saf 81(1):23–69

Huu VH, Duong-Gia D, Vo-Duy T, Le-Duc T (2018) Nguyen-Thoi, an efficient combination of multi-objective evolutionary optimization and reliability analysis for reliability-based design optimization of truss structures. Expert Syst Appl 102:262–272

Hvejsel CF, Lund E (2011) Material interpolation schemes for unified topology and multi-material optimization. Struct Multidiscip Optim 43(6):811–825

Imani M, Ghoreishi SF, Braga-Neto UM (2018) Bayesian control of large MDPs with unknown dynamics in data-poor environments. Adv Neural Inf Proces Syst:8146–8156

Imani M, Ghoreishi SF, Allaire D, Braga-Neto UM (2019) MFBO-SSM: multi-fidelity Bayesian optimization for fast inference in state-space models. Proc AAAI Conf Artif Intell 33:7858–7865

Jeong SB, Park GJ (2017) Single loop single vector approach using the conjugate gradient in reliability based design optimization. Struct Multidiscip Optim 55(4):1329–1344

Jung Y, Cho H, Lee IJ (2019) MPP-based approximated DRM (ADRM) using simplified bivariate approximation with linear regression. Struct Multidiscip Optim 59(5):1761–1773

Kang SB, Park JW, Lee IJ (2017) Accuracy improvement of the most probable point-based dimension reduction method using the hessian matrix. Int J Numer Methods Eng 111(3):203–217

Lee IJ, Choi KK, Du L, Gorsich D (2008) Inverse analysis method using MPP-based dimension reduction for reliability-based design optimization of nonlinear and multi-dimensional systems. Comput Methods Appl Mech Eng 198(1):14–27

Lee IJ, Choi KK, Gorsich D (2010) Sensitivity analyses of FORM-based and DRM-based performance measure approach (PMA) for reliability-based design optimization (RBDO). Int J Numer Methods Eng 82(1):26–46

Lee IJ, Noh Y, Yoo D (2012) A novel second-order reliability method (SORM) using noncentral or generalized chi-squared distributions. J Mech Des 134(10):100912

Liu L, Yan J, Cheng GD (2008) Optimum structure with homogeneous optimum truss-like material. Comput Struct 86(13):1417–1425

Ma XT, Tian K, Li HQ, Zhou Y, Hao P, Wang B (2020) Concurrent multi-scale optimization of hybrid composite plates and shells for vibration. Compos Struct 233:111635

Mallick PK (2007) Fiber-reinforced composites: materials, manufacturing, and design. CRC press

Lund E (1994) Finite element based design sensitivity analysis and optimization. Institute of Mechanical Engineering, Aalborg University, Denmark

Martins LAL, Bastian FL, T.A. (2014) Netto, reviewing some design issues for filament wound composite tubes. Mater Des 55:242–249

Niu B, Yan J, Cheng GD (2009) Optimum structure with homogeneous optimum cellular material for maximum fundamental frequency. Struct Multidiscip Optim 39(2):115–132

Papadrakakis M, Lagaros ND (2002) Reliability-based structural optimization using neural networks and Monte Carlo simulation. Comput Methods Appl Mech Eng 191(32):3491–3507

Rodrigues H, Guedes JM, Bendsøe M (2002) Hierarchical optimization of material and structure. Struct Multidiscip Optim 24(1):1–10

Rosenblatt M (1952) Remarks on a multivariate transformation. Ann Math Stat 23:470–472

Shin JW, Lee IJ (2014) Reliability-based vehicle safety assessment and design optimization of roadway radius and speed limit in windy environments. J Mech Des 136.8

Sohouli A, Yildiz M, Suleman A (2018) Efficient strategies for reliability-based design optimization of variable stiffness composite structures. Struct Multidiscip Optim 57(2):689–704

Sørensen SN, Sørensen R, Lund E (2014) DMTO–a method for discrete material and thickness optimization of laminated composite structures. Struct Multidiscip Optim 50(1):25–47

Stegmann J, Lund E (2005) Discrete material optimization of general composite shell structures. Int J Numer Methods Eng 62(14): 2009–2027

Shimoda M, Nagano T, Shi JX (2019) Non-parametric shape optimization method for robust design of solid, shell, and frame structures considering loading uncertainty. Struct Multidiscip Optim 59(5): 1543–1565

Wu C, Gao YK, Fang JG, Lund E, Li Q (2019) Simultaneous discrete topology optimization of ply orientation and thickness for carbon Fiber reinforced plastic-laminated structures. J Mech Des 141(4): 044–501

Xu YN, Gao YK, Wu C, Fang JG, Li Q (2019) Robust topology optimization for multiple fiber-reinforced plastic (FRP) composites under loading uncertainties. Struct Multidiscip Optim 59(3):695–711

Xie SL, Imani M, Dougherty ER, Braga-Neto UM (2017) Nonstationary linear discriminant analysis. 51st Asilomar Conference on Signals, Systems, and Computers, Pacific Grove, CA, pp 161–165

Yan J, Duan ZY, Lund E, Wang JY (2017) Concurrent multi-scale design optimization of composite frames with manufacturing constraints. Struct Multidiscip Optim 56(3):519–533

Yan J, Cheng GD, Liu L (2008) A uniform optimum material based model for concurrent optimization of thermoelastic structures and materials. Int J Simul Multidiscip Des Optim 2(4):259–266

Yang DX, Yi P (2009) Chaos control of performance measure approach for evaluation of probabilistic constraints. Struct Multidiscip Optim 38:83–92

Yang DX, Li XL, Chen GH (2018) Accelerated stability transformation method for chaos control of discrete dynamical systems. Nonlinear Dyn 94(2):1195–1213

Youn BD, Choi KK, Park YH (2003) Hybrid analysis method for reliability-based design optimization. J Mech Des 125(2):221–232

Meng Z, Gang L, Wang BP, Hao P (2015) A hybrid chaos control approach of the performance measure functions for reliability-based design optimization. Comput Struct 146:32–43

Duan ZY, Yan J, Lee IJ, Lund E, Wang JY (2019b) Discrete material selection and structural topology optimization of composite frames for maximum fundamental frequency with manufacturing constraints. Struct Multidiscip Optim 60(5):1741–1758

Zuo ZH, Huang XD, Rong JH, Xie YM (2013) Multi-scale design of composite materials and structures for maximum natural frequencies. Mater Des 51:1023–1034